Remote Sensing of Environment 264 (2021) 112607

Contents lists available at ScienceDirect

Remote Sensing of Environment

journal homepage: www.elsevier.com/locate/rse

Spectral variations of the remote sensing reflectance during coccolithophore blooms in the Western Black Sea

Ilaria Cazzaniga *, Giuseppe Zibordi, Frédéric Mélin

European Commission, Joint Research Centre (JRC), Ispra, Italy

ARTICLE INFO

Keywords:
Remote sensing
Ocean color
Coccolithophores
Phytoplankton
Radiometry
Satellite
Remote sensing reflectance

ABSTRACT

Among the many calcifying marine organisms, coccolithophores are the major producer of particulate inorganic carbon (*PIC*). Calcium carbonate plates covering coccolithophores, called coccoliths and released during blooms, are responsible for a large increase of the water reflectance. Aiming at investigating the spectral features of the remote sensing reflectance $R_{RS}(\lambda)$ of marine waters during coccolithophore blooms, this study exploits the radiometric data of Ocean Color sites of the Aerosol Robotic Network (AERONET-OC) in the Western Black Sea (Galata and Gloria/Section-7) by focusing on bloom events that occurred in 2017 and 2020. The analysis, besides showing elevated $R_{RS}(\lambda)$ in the blue-green spectral region in the presence of coccoliths, confirms a shift toward the blue of the $R_{RS}(\lambda)$ spectra as the bloom declines and coccoliths accumulate at the surface. Results also document a decreased capability of determining the bloom state in the presence of optically complex waters such as those associated with river runoff. Finally, the comparison of satellite versus AERONET-OC radiometric data for the extreme conditions created by the presence of coccolithophores, indicates agreements between $R_{RS}(\lambda)$ not significantly different from those previously determined for various satellite data products in the absence of appreciable concentrations of coccoliths.

1. Introduction

Coccolithophores are eukaryotic unicellular phytoplankton with an exoskeleton made of individual plates of calcium carbonate called coccoliths. Among the many calcifying marine organisms, coccolithophores are the major producer of particulate inorganic carbon (*PIC*) that significantly influences the carbon balance and consequently impacts global biogeochemical cycles over short and geological time scales (Balch et al., 2011; Müller, 2019). Dedicated studies (e.g., Thierstein and Young, 2013) investigated the life cycle, global distribution and phenology of these organisms among which *Emiliania huxleyi* is the most spread species throughout latitude (Holligan and Balch, 1991). These investigations largely benefitted of remote sensing technologies exploiting the increase of the water reflectance due to the high scattering of coccolithophores and their detached coccoliths. Specifically, current algorithms use the spectral normalized water-leaving radiance $L_{WN}(\lambda)$ or alternatively the spectral remote-sensing reflectance $R_{RS}(\lambda)$ to detect the presence of coccoliths (Iglesias-Rodríguez et al., 2002; Moore et al., 2012), estimate the back-scattering coefficient of particulate matter $b_{bp}(\lambda)$, and, from this, the concentration of coccoliths and *PIC* concentrations (Balch et al., 2005; Gordon et al., 2001). Recent investigations proposed the direct application of $R_{RS}(\lambda)$ to determine *PIC* concentration (Mitchell et al., 2017).

Several studies investigated the evolution and distribution of coccolithophore blooms through remote sensing techniques by using Coastal Zone Color Scanner (CZCS) and Sea-viewing Wide Field-of-view Sensor (SeaWiFS) imagery (Balch et al., 2018; Brown and Yoder, 1994; Cokacar et al., 2001; Holligan and Balch, 1991; Hopkins et al., 2015; Kopelevich et al., 2014). With specific reference to the Black Sea, which is the region of interest in this study, SeaWiFS time-series for the period 1998–2002 showed an evident coincidence between the so called June maximum of the water-leaving radiance and coccolithophore blooms (Karabashev et al., 2006). Additionally, ocean color imagery from SeaWiFS, Ocean Color and Temperature Scanner (OCTS) and Moderate Resolution Imaging Spectroradiometer (MODIS) showed an almost regular yearly occurrence of coccolithophore blooms between May and June (Cokacar et al., 2004; Cokacar et al., 2001; Kopelevich et al., 2014; Korchemkina et al., 2019). On the quantitative side, Kopelevich et al. (2014) proposed a regional algorithm for the Black Sea based on a relationship between coccoliths concentration and $b_{bp}(\lambda)$. More recently,

* Corresponding author.
E-mail address: ilaria.cazzaniga@ec.europa.eu (I. Cazzaniga).

https://doi.org/10.1016/j.rse.2021.112607
Received 24 November 2020; Received in revised form 10 July 2021; Accepted 12 July 2021
Available online 10 August 2021

benefitting from the R/V Professor Vodyanitsky expedition carried out in the Black Sea during the 2017 coccolithophore bloom, Korchemkina et al. (2019) exploited field measurements of the beam attenuation coefficient to investigate the bio-optical characteristics of coccolithophores and addressed the accuracy of coccoliths concentrations from a semi-analytical algorithm applied to MODIS derived $R_{RS}(\lambda)$.

Regardless of the former extensive investigations, there are very few in situ reflectance spectra related to coccolithophore blooms documented in the literature (e.g., Garcia et al., 2011; Iida et al., 2002; Smyth et al., 2002). For this reason, algorithms dedicated to coccolithophore blooms identification are based on satellite sensor derived reflectance from different regions around the globe (e.g., Brown and Yoder, 1994; Iglesias-Rodríguez et al., 2002; Moore et al., 2012), not including the Black Sea. Exception is the work by Slabakova et al. (2020) on the assessment of the Ocean and Land Color Instrument (OLCI) radiometric products in the Western Black Sea, still not focusing on coccolithophore blooms but embracing periods characterized by blooms.

This study relies on an unprecedented description of coccolithophore blooms offered by time-series of in situ measurements performed by autonomous multispectral radiometers located in the Western Black Sea and belonging to the Ocean Color component of the Aerosol Robotic Network (AERONET-OC, Zibordi et al., 2009). Its main objectives are to investigate the $R_{RS}(\lambda)$ spectral features in the 400–700 nm interval and their variability in relation to the temporal evolution of coccolithophore blooms, and to evaluate current algorithms for coccolithophore blooms detection in the Black Sea. As an additional objective, the study aims at assessing the accuracy of remote sensing radiometric products from ocean color sensors from various satellite missions in the presence of coccoliths, which has been little documented so far. In fact, the strong backscattering due to the presence of coccoliths is not specifically accounted for by current atmospheric correction schemes, potentially challenging the accurate retrieval of $L_{WN}(\lambda)$ or $R_{RS}(\lambda)$, and consequently the performance of the algorithms for coccoliths detection and the determination of *PIC* concentration.

1.1. Study area and measurement sites

The Black Sea is a semi-enclosed sea whose catchment basin is approximately five times larger than its area. It receives drainage from almost one-third of the European rivers through the Danube, Dniester and Dnieper whose waters exhibit high concentrations of nitrogen and phosphorus nutrients (Vespremeanu and Golumbeanu, 2018). The

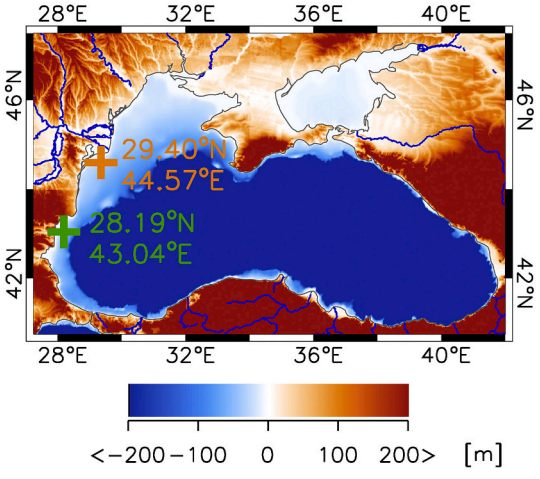

Fig. 1. Study area: bathymetry map and AERONET-OC sites location. The green and orange crosses indicate the Galata and Gloria/Section-7 sites, respectively. For Gloria/Section-7 the mean values of the coordinates between the two sites are indicated. (For interpretation of the references to color in this figure legend, the reader is referred to the web version of this article.)

north-western shelf region, of relevance for this study, exhibiting depths lower than 200 m (see Fig. 1), receives approximately 80% of the freshwater runoff discharged in the Black Sea (Aubrey et al., 1996).

Considering a Black Sea regional partition as a function of bathymetry and river runoff (Kopelevich et al., 2014), the AERONET-OC sites relevant for the study (i.e., Galata and Gloria/Section-7, see Fig. 1) are located in the north-western and south-western inner shelves. These regions are both characterized by high variability of their optically complex waters (Zibordi et al., 2015) as a result of the combined influence of the local dynamics and discharge of the Danube, Dnieper, Dniester and Bug rivers.

The Gloria AERONET-OC site (Lon. 29.36°E, Lat. 44.60°N), established in 2010 on the homonymous gas platform owned and managed by the *Petrom* company, is located at approximately 12 nautical miles from the Romanian coast south of the Danube mouth. In August 2019, this site was decommissioned and replaced by Section-7 (Lon. 29.45°E, Lat. 44.45°N), a gas platform also owned and managed by *Petrom* and located a few nautical miles south of Gloria. The water depth at the two locations is approximately 40 m.

The Galata AERONET-OC site (Lon. 28.19°E, Lat. 43.05°N) established in 2014 on the homonymous gas platform owned and managed by the *Melrose* company, is located at approximately 13 nautical miles off the Bulgarian coast in front of the city of Varna. The water depth at this site is 35 m.

As already documented, the Western Black Sea exhibits almost regular yearly occurrence of coccolithophore blooms developing during June and usually gradually vanishing through July (Kopelevich et al., 2014). However, the shelf regions were not always included in previous coccolithophore investigations relying on satellite data (e.g., Cokacar et al., 2004; Cokacar et al., 2001). The shelf areas with depth lower than 200 m, indeed, are largely affected by the presence of particulate and dissolved matter from river runoff. This enhanced optical complexity may challenge the capability to detect coccoliths through ocean color techniques. Based on the time-series from 1991 to 2008, Danube runoff typically shows its peak between the end of April and the beginning of May (Stagl and Hattermann, 2015), when coccolithophore blooms may already occur (Kubryakov et al. (2019)).

2. Materials and methods

2.1. AERONET-OC data

AERONET-OC was conceived to support ocean color activities with $L_{WN}(\lambda)$ and aerosol optical depth τ_a data retrieved from autonomous radiometer systems (Zibordi et al., 2009, 2021). AERONET-OC gathers field measurements from CE-318 and CE-318T radiometers deployed on fixed offshore structures and allows for their near real-time data processing and archival at different quality levels (i.e., Level 1.0, Level 1.5 and Level 2.0). AERONET-OC CE-318 radiometers have up to 9 spectral bands in the 412–1020 nm interval largely overlapping with MODIS and the Visible Infrared Imaging Radiometer Suite (VIIRS) bands (for instruments deployed in 2017 at both sites, nominal center-wavelengths were 412, 443, 490, 532, 551, 667, 870, 1020 nm). Conversely, AERONET-OC CE-318T radiometers, which have been deployed since 2018, have up to 12 spectral bands in the 400–1020 nm interval matching most of the OLCI ones. For marine sites, including Galata and Section-7, the relevant center-wavelengths are 400, 412, 443, 490, 510, 560, 620, 667, 779, 865, 1020 nm. In addition to an increased number of spectral bands, CE-318T systems offer the capability of performing replicate (typically three successive) sequences of measurements, thus delivering multiple $L_{WN}(\lambda)$ retrievals contrary to the single one permitted by CE-318 systems every 30 min. Definitively, the capability of performing a higher number of measurements allows for better addressing the temporal evolution of short-term events (i.e., at the scale of a few minutes). Gergely and Zibordi (2014) reported relative uncertainties for $L_{WN}(\lambda)$ for the Gloria site approaching 5–6% in the blue-

green spectral region and 10% in the red. These uncertainties are expected to also apply to Section-7 and Galata $L_{WN}(\lambda)$.

Details on AERONET-OC instruments and recent advances in measurement protocols and data processing, are comprehensively described in Zibordi et al. (2021).

This study relies on AERONET-OC Level-2 fully quality checked $L_{WN}(\lambda)$ data in units of mW cm^{-2} μm^{-1} sr^{-1}, with λ indicating the center-wavelength of each spectral band (hereafter provided in units of nm). Exceptions are the $L_{WN}(\lambda)$ data for the year 2020 for which Level 1.5 only was accessible when this study was performed. Level 2.0 data, indeed, are available with some delay: they are derived from Level 1.5 data, but require final radiometric adjustments associated with the post-deployment calibration of field instruments and a final spectrum-by-spectrum screening performed by an experienced scientist.

AERONET-OC $L_{WN}(\lambda)$ data, corrected for bidirectional effects applying the scheme proposed by Morel et al. (2002), were used. $R_{RS}(\lambda)$ in units of sr^{-1}, were derived from $L_{WN}(\lambda)$ through:

$$R_{RS}(\lambda) = \frac{L_{WN}(\lambda)}{F_0(\lambda)} \tag{1}$$

with $F_0(\lambda)$ the spectral mean extra-atmospheric irradiance, in units of mW cm^{-2} μm^{-1}, from Thuillier et al. (2003).

The Gloria and Section-7 data, which refer to contiguous periods and nearby sites, were considered as a single time-series.

2.2. Events identification and analysis

Coccolithophore bloom events have been investigated exploiting spectral features resulting from coccoliths scattering through an algorithm initially proposed for CZCS and SeaWiFS imagery (Iglesias-Rodríguez et al., 2002). This algorithm sets a flag, hereafter called coccoliths flag, on the basis of thresholds applied to spectral values of $L_{WN}(\lambda)$ and their ratios:

$$coccoliths\ flag = \begin{cases} \text{ON} & if \begin{cases} L_{WN}(443) > 1.1 \\ L_{WN}(555) >= 0.9 \\ 0.75 < R1 < 1.85 \\ 1.0 < R2 < 1.65 \\ 0.6 < R3 < 1.15 \end{cases} \\ \text{OFF} & otherwise \end{cases} \tag{2}$$

where

$$R1 = \frac{L_{WN}(443)}{L_{WN}(555)} \tag{3}$$

$$R2 = \frac{L_{WN}(510)}{L_{WN}(555)} \tag{4}$$

$$R3 = \frac{L_{WN}(443)}{L_{WN}(510)} \tag{5}$$

The algorithm, as coded into the NASA's Ocean Color processor (l2gen of the SeaWiFS Data Analysis System, SeaDAS (Baith et al., 2001)), is currently applied to MODIS and VIIRS data, where $L_{WN}(510)$ is replaced by $L_{WN}(531)$ or $L_{WN}(489)$, respectively, acknowledging its potentially lower effectiveness (Moore et al., 2012). Consistently, in this study the coccoliths flag algorithm was applied to OLCI products and to AERONET-OC $L_{WN}(\lambda)$ using $L_{WN}(530)$, when $L_{WN}(510)$ was not available, and also replacing $L_{WN}(555)$ with $L_{WN}(551)$ or alternatively with $L_{WN}(560)$, depending on the data source.

The determination of *PIC* in units of mol m^{-3} was obtained using the Color Index (*CI*) algorithm (Mitchell et al., 2017), recognizing that its validity for optically complex waters is still under investigation. *PIC* is determined from:

$$PIC = 0.4579\ CI - 0.0006 \tag{6}$$

with

$$CI = R_{RS}(547) - R_{RS}\ (667) \tag{7}$$

When required, the values of satellite or AERONET-OC $R_{RS}(547)$ and $R_{RS}(667)$ were determined from $R_{RS}(\lambda)$ (with λ indicating the closest available center-wavelength) through the band-shift technique based on regional bio-optical algorithms developed using in situ data from the Western Black Sea (Zibordi et al., 2015). The band-shift corrections were also applied to AERONET-OC $R_{RS}(\lambda)$ data used for matchups (i.e., nearly contemporaneous in situ and satellite data pairs) to minimize the impact of spectral differences between in situ and satellite center-wavelengths. It is however acknowledged that the uncertainty associated with these corrections applied to data from optically complex waters dominated by the presence of coccoliths may be quite large.

While recognizing the unique value of the AERONET-OC time-series at the two locations spanning across several years, the study focused on the 2017 and 2020 coccolithophore events because of their intensity and duration. These recent events, indeed, exhibited a spatial distribution embracing both AERONET-OC locations with duration exceeding three months in 2017 and approaching two months in 2020. Additionally, the availability of CE-318T 12-band data during the 2020 event offered access to more spectrally resolved $L_{WN}(\lambda)$, compared to the corresponding products from the CE-318 9-band radiometers used in 2017.

The occurrence of the 2017 event was confirmed through in situ measurements by Kopelevich et al. (2020) and Korchemkina et al. (2019) in the Northern and Eastern Black Sea, and by Slabakova et al. (2020) in the Western Black Sea. For the 2020 event, confidence on the presence of coccolithophore blooms in the region was heuristically provided by $R_{RS}(\lambda)$ well above background values and the typical milky turquoise aspect of waters in true-color satellite images.

2.3. Satellite data processing and satellite-derived $R_{RS}(\lambda)$ validation

$R_{RS}(\lambda)$ from standard ocean color products, as distributed by space agencies, were evaluated. These products are associated with the following sensors: MODIS on board the Aqua and Terra platforms (MODIS-A, and MODIS-T, Esaias et al., 1998), VIIRS on board the Suomi National Polar-orbiting Partnership (VIIRS-SNPP) and the Joint Polar Satellite System 1 (VIIRS-JPSS, Goldberg et al., 2013; Schueler et al., 2002), and OLCI operated on board the Sentinel-3A platform (OLCI-A, Donlon et al., 2012).

Level-1A data from MODIS-A, MODIS-T, VIIRS-SNPP and VIIRS-JPSS for the area of interest were processed with the atmospheric correction l2gen embedded in the version 7.5 of SeaDAS (Franz et al., 2007 and references therein). The resulting Level-2 data are consistent with NASA's Ocean Biology Processing Group (OBPG) Reprocessing R2018 and the latest calibration table. Data from OLCI-A were obtained as Level-2 Reduced-Resolution (1.2-km) products from the European Organisation for the Exploitation of Meteorological Satellites (EUMETSAT) Data Centre (EUMETSAT, 2018, Processing Baseline 2.23 and successive revisions up to 2.58), and corrected for bidirectional effects using the same scheme that was applied to AERONET-OC data.

Both the EUMETSAT (Antoine, 2010; Moore and Lavender, 2010) and NASA (Gordon and Wang, 1994; Ahmad et al., 2010; Bailey et al., 2010) atmospheric correction schemes rely on the black pixel assumption, including corrections for non-black pixels in the near-infrared (NIR) spectral region. The correction applied to MODIS and VIIRS data is based on an iterative process leading to the determination of $R_{RS}(\lambda)$ in the NIR through the IOP-based method detailed in Bailey et al. (2010). The alternative method implemented for OLCI, instead, applies a correction based on the similarity spectrum detailed in Moore and Lavender (2010).

The vicarious calibration gains (i.e., *g*-factors) required to minimize

the effects of biases affecting the calibration of the space sensor and the models embedded in the atmospheric correction, were determined for either MODIS, VIIRS and OLCI relying on the method proposed by Franz et al. (2007). However, while the NIR *g*-factors were equally determined by the two institutions using observations over the South Pacific Gyre, the determination of the *g*-factors for the visible spectral bands requiring in situ reference measurements is marked by differences. MODIS and VIIRS processing benefitted of *g*-factors determined with reference data from the Marine Optical Buoy (MOBY, Clark et al., 2003). Conversely, OLCI-A processing relied on a temporary solution using a variety of in situ measurements and the GlobColour climatology (EUMETSAT, 2017).

It is emphasized that none of the processors benefits of specific implementations supporting atmospheric corrections in the presence of coccolithophore blooms.

For each macro-pixel made of the 3 × 3 image elements centered at each AERONET-OC site, the median of the $R_{RS}(\lambda)$ values was calculated excluding data affected by the standard processing flags. For the NASA data products (i.e., MODIS and VIIRS), the exclusion flags used in this study were: 'ATMFAIL', 'LAND', 'HIGLINT', 'HILT', 'HISATZEN', 'STRAYLIGHT', 'CLDICE', 'HISOLZEN', 'LOWLW', 'CHLFAIL', 'NAVWARN', 'MAXAERITER', 'CHLWARN', 'ATMWARN', 'NAVFAIL' (except for 'COCCOLITH', the above flags are those recommended by NASA for global processing).

For the EUMETSAT data products (i.e., OLCI-A) the exclusion flags were: 'CLOUD', 'CLOUD_AMBIGUOUS', 'CLOUD_MARGIN', 'INVALID', 'COSMETIC', 'SATURATED', 'SUSPECT', 'HISOLZEN', 'HIGHGLINT', 'SNOW_ICE', 'AC_FAIL', 'WHITECAPS', 'RWNEG_O2', 'RWNEG_O3', 'RWNEG_O4', 'RWNEG_O5', 'RWNEG_O6', 'RWNEG_O7', 'RWNEG_O8'.

Two analyses were performed: one including those matchups affected by the presence of coccoliths during the two blooms; and the other including all available matchups since 2018, but not affected by coccoliths. It is specified that the presence of coccoliths was established through the application of the coccoliths flag to AERONET-OC data. On the contrary, for time-series of satellite data products, the presence of coccoliths was determined from the satellite data themselves using the embedded coccoliths flag in NASA products, or alternatively calculated for OLCI-A data.

Adopting an approach similar to previous works (e.g., Mélin et al., 2011), in situ – satellite matchups were constructed using the following criteria: (a) the time difference between the acquisition time of AERONET-OC data and satellite overpass was lower than 2 h; (b) none of the 9 pixels in the macro-pixel was flagged by exclusion flags; (c) the coefficient of variation (*CV*, i.e., the ratio of macro-pixel standard deviation and average) at 560 nm (or equivalent center-wavelength) was lower than 20%.

For each site and sensor, the root mean square difference RMSD, mean relative difference ψ and mean absolute relative difference $|\psi|$, were determined from the available matchups as:

$$\mathrm{RMSD} = \sqrt{\frac{1}{N}\sum_{i=1}^{N}\left(x_i^S - x_i^A\right)^2} \tag{8}$$

$$\psi = \frac{1}{N}\sum_{i=1}^{N}\frac{\left(x_i^S - x_i^A\right)}{x_i^A}\ 100 \tag{9}$$

$$|\psi| = \frac{1}{N}\sum_{i=1}^{N}\frac{\left|x_i^S - x_i^A\right|}{x_i^A}\ 100 \tag{10}$$

where N is the number of matchups, x_i^S indicates satellite-derived $R_{RS}(\lambda)$ and x_i^A the AERONET-OC $R_{RS}(\lambda)$ at corresponding center-wavelengths.

These statistical indices summarize the observed differences in terms of scatter and systematic difference (bias), in both relative terms (%) and units of $R_{RS}(\lambda)$. These indices are commonly used by the ocean color community to describe results from matchup analysis and were also adopted in this work to make results comparable across independent studies. It is fully acknowledged that the use of percent differences (relying on field data as the reference) instead of unbiased-percent differences, may lead to unrealistic values in the presence of $R_{RS}(\lambda)$ close to zero. The regression slope m, intercept q and determination coefficient r^2 were also computed through linear least-squares regressions.

The matchups identified in the former statistical analysis were also used to compare *PIC* determined from satellite $R_{RS}(\lambda)$ with those from AERONET-OC $R_{RS}(\lambda)$. It is stressed that this is not a validation of satellite products for *PIC* (for which in situ data are not available), but a quantification of how differences between field and satellite $R_{RS}(\lambda)$ data propagate into the determination of *PIC*.

3. Results

3.1. Temporal evolution of the 2017 and 2020 coccolithophore blooms in the Western Black Sea

The analysis of AERONET-OC data shows the occurrence of coccolithophore blooms at both AERONET-OC locations during recent spring-summer periods (Table 1). The duration of each bloom was determined yearly by the interval between the first and the last occurrence of raised coccoliths flag as determined from AERONET-OC data during the spring-summer period. It should be noted that the correct identification of the start and end dates is conditioned by data availability and, additionally, by perturbations from estuarine optically complex waters that may mask the coccoliths scattering (see the case of May 2017 discussed later in Section 3.4). Table 1 also shows the *PIC* values at the start and end dates of the bloom: high *PIC* values at the start date may indicate that the bloom is already occurring and consequently a failure of the coccoliths flag (e.g., see the Gloria site during 2017).

Bloom intervals based on the outcome from the coccoliths flag were also derived from satellite-sensors data during spring-summer of each year. As an example, Table 2 indicates the blooms duration in 2017 and 2020. Excluding exceptions (e.g., the first activation for VIIRS-JPSS and OLCI-A in 2020 at Galata), satellite-based and AERONET-OC determinations describe a fairly consistent picture of bloom evolutions. It is however noted, and later addressed in Section 4, that false negatives, as well as different sensor band-settings and data availability may affect satellite outputs. Finally, when comparing satellite and AERONET-OC determinations, differences in measurement frequency and spatial resolution may also influence results, particularly in regions characterized by high temporal and spatial variability.

Fig. 2 displays the temporal evolution of AERONET-OC $R_{RS}(\lambda)$ at selected bands and satellite derived $R_{RS}(490)$ at the two sites during the 2017 and 2020 coccolithophore blooms. In correspondence with each

Table 1
Coccolithophore bloom events occurring since 2015 in the Western Black Sea as identified through the coccoliths flag determined from AERONET-OC data from Galata and Gloria/Section-7. The *PIC* values associated with the first and the last activation dates are also shown.

Year	Period (Galata)	Period (Gloria/ Section-7)	*PIC* at start (10^{-3} mol m^{-3})		*PIC* at end (10^{-3} mol m^{-3})	
			Galata	Gloria/ Section-7	Galata	Gloria/ Section-7
2015	11 July - 28 July	26 July - 30 July	3	1.8	1.7	1.6
2016	30 May - 18 June	19 June - 25 June	3.7	3.8	3.1	3.7
	4 July - 7 July		1.6		2.3	
2017	7 May - 11 August	25 June - 9 August	2.2	6.4	1.7	2.1
2018	–	–	–	–	–	–
2019	23 May - 14 June	–	2.3	–	1.8	–
2020	30 April - 23 June	10 May - 28 June	2.2	6.3	1.6	3.4

Table 2
Coccolithophore bloom events duration in 2017 and 2020 as identified by coccoliths flag, for each sensor and site.

SITE	YEAR	VIIRS-SNPP	VIIRS-JPSS	MODIS-A	MODIS-T	OLCI-A
Galata	**2017**	11 May - 4 August	Not available	11 May - 10 August	11 May - 6 August	16 May - 16 August
	2020	30 April - 20 June	24 May - 18 June	1 May - 22 June	30 April - 20 June	24 May - 12 June
Gloria/	**2017**	24 June - 8 August	Not available	23 June - 5 August	23 June - 3 August	28 June - 2 August
Section-7	**2020**	5 May - 28 June	11 May - 29 June	5 May - 29 June	8 May - 4 July	21 May - 4 July

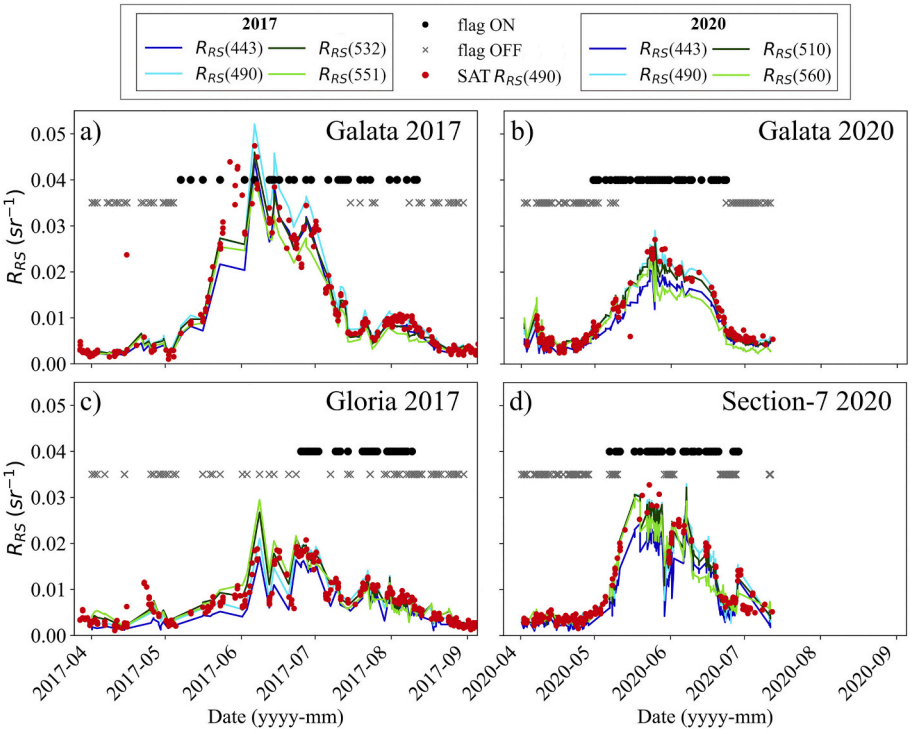

Fig. 2. AERONET-OC $R_{RS}(\lambda)$ data as a function of time at selected center-wavelengths from (a,b) Galata and (c,d) Gloria/Section-7 for the (a,c) 2017 and (b,d) 2020 coccolithophore events. The black • and grey × symbols indicate the values ON (raised) and OFF (not raised), respectively, of the coccoliths flag for each AERONET-OC measurement. The red dots indicate satellite derived $R_{RS}(\lambda)$ at 490 nm (or at an equivalent center-wavelength) for MODIS-T, MODIS-A, VIIRS-JPSS, VIIRS-SNPP and OLCI-A. (For interpretation of the references to color in this figure legend, the reader is referred to the web version of this article.)

bloom period, as identified by the coccoliths flag shown by black dots, high reflectance values are observed. The 2017 event, that tentatively occurred from May 7th through August 11th (as determined using AERONET-OC data from Galata), was characterized by the highest $R_{RS}(490)$ values. An extremely high reflectance determined with MODIS-A and MODIS-T was also documented by Korchemkina et al. (2019) who reported values ten times higher than the seasonal mean in the north-western Black Sea. In 2020, according to the AERONET-OC data from both Galata and Section-7, the bloom event occurred from at least April 30th through June 28th.

During both the 2017 and 2020 events (see Fig. 2), satellite data closely reproduce the temporal evolution of the blooms determined with

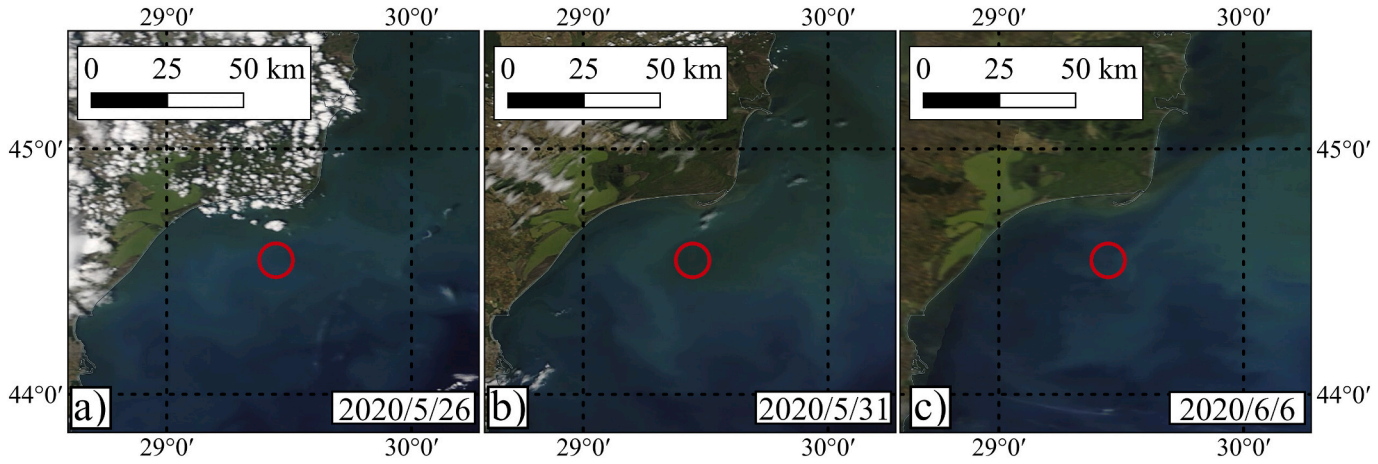

Fig. 3. True color MODIS-T images of May 26th, May 31st and June 6th 2020. The red circles identify the region centered on Section-7. The true color images were generated through EOSDIS worldview with corrected reflectance products using the MODIS bands 1, 4 and 3 for the red, green and blue, respectively (see https://earthdata.nasa.gov/faq/worldview-snapshots-faq#modis-true-color for products description). Turquoise waters are indicative of coccolithophore blooms. (For interpretation of the references to color in this figure legend, the reader is referred to the web version of this article.)

AERONET-OC data at both locations. Exceptions are a few outliers appearing in OLCI-A data (e.g., see panels a and b), likely caused by cloud contamination not captured by the relevant flags.

It is also noted that in some periods the coccoliths flag is irregularly activated. At Galata, this is particularly evident at the beginning and end of the bloom and is likely explained by fluctuations in the concentration of coccoliths. Conversely, at Gloria/Section-7 the abrupt changes characterizing the coccoliths flag during the evolution of blooms are more likely explained by the impact of the Danube waters, rich of sediments and organic dissolved matter affecting the $R_{RS}(\lambda)$ spectra. This is illustrated by Fig. 3 through successive MODIS-T corrected reflectance true color images generated with EOSDIS worldview (see description of data products at https://earthdata.nasa.gov/faq/worldview-snapshots-faq). The image of May 31st 2020, opposite to those of May 26th and June 6th, indicates green-brownish waters from the Danube mouths affecting the region surrounding Section-7. The analysis of the coccoliths flag determined from AERONET-OC indicates it was 'OFF' on May 31st, and 'ON' on May 26th and June 6th, when the water nearby Section-7 exhibits the turquoise color typical of coccolithophore blooms.

3.2. Spatial distribution of the 2017 and 2020 coccolithophore blooms in the Western Black Sea

As already anticipated for Fig. 3, evidence of the occurrence of coccolithophore blooms during the periods identified by AERONET-OC data is distinctly provided by satellite observations. Fig. 4 shows a selection of VIIRS-SNPP corrected reflectance true color images. They qualitatively show, as indicated by the turquoise waters, the spatial distribution of the coccolithophore blooms at different dates during the 2017 and 2020 events. Notably, the shelf regions including the location of the AERONET-OC sites were particularly impacted during both events. In 2017, as shown by the image of June 23rd, the bloom involved almost the whole basin. During its final stage, it only affected the northwestern region. During 2020, when compared to 2017, the spatial extent

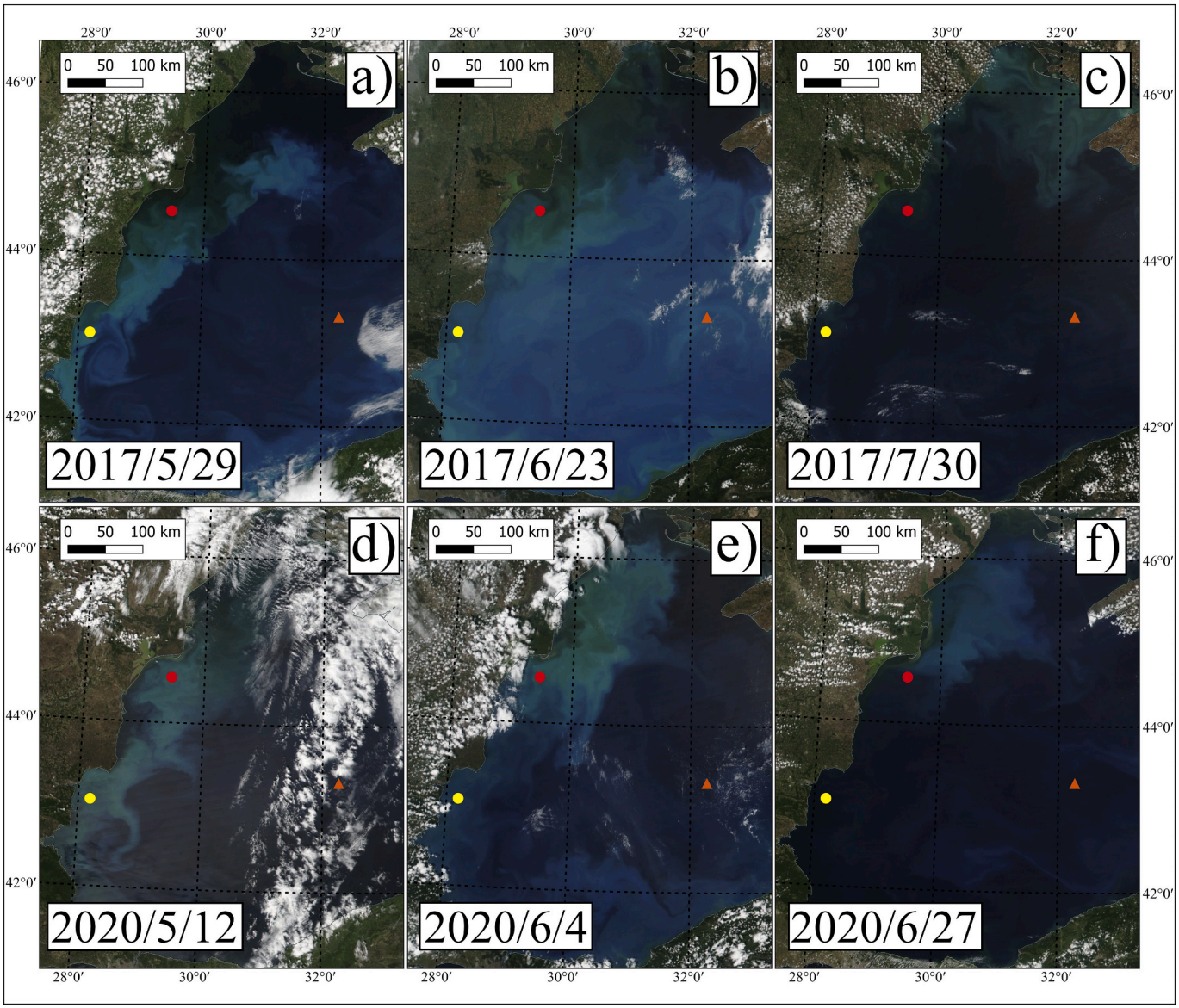

Fig. 4. True color VIIRS-SNPP imagery showing the spatial distribution of the 2017 and 2020 coccolithophore blooms in the Western Black Sea at different dates. The true color images were generated through EOSDIS worldview with corrected reflectance products using the VIIRS-SNPP bands I1, M4 and M3 for the red, green and blue respectively (see https://earthdata.nasa.gov/faq/worldview-snapshots-faq#snpp-true-color for products description). Dots indicate the Gloria/Section-7 and Galata sites in red and yellow, respectively. The triangle indicates a location in the Central Black Sea referred to in Section 4. (For interpretation of the references to color in this figure legend, the reader is referred to the web version of this article.)

of the bloom was less pronounced and the central part of the basin was much less affected than the western and southern regions. Similar to 2017, the 2020 bloom only occupied the north-western region during its final stage.

3.3. Assessment of satellite-derived $R_{RS}(\lambda)$ during coccolithophore blooms

A quantitative application of satellite ocean color data in marine regions affected by coccolithophore blooms requires an assessment of their primary radiometric products: $L_{WN}(\lambda)$ or alternatively $R_{RS}(\lambda)$. Benefitting of the in situ reference data from the Black Sea AERONET-OC sites, this section aims at providing an assessment of $R_{RS}(\lambda)$ data affected

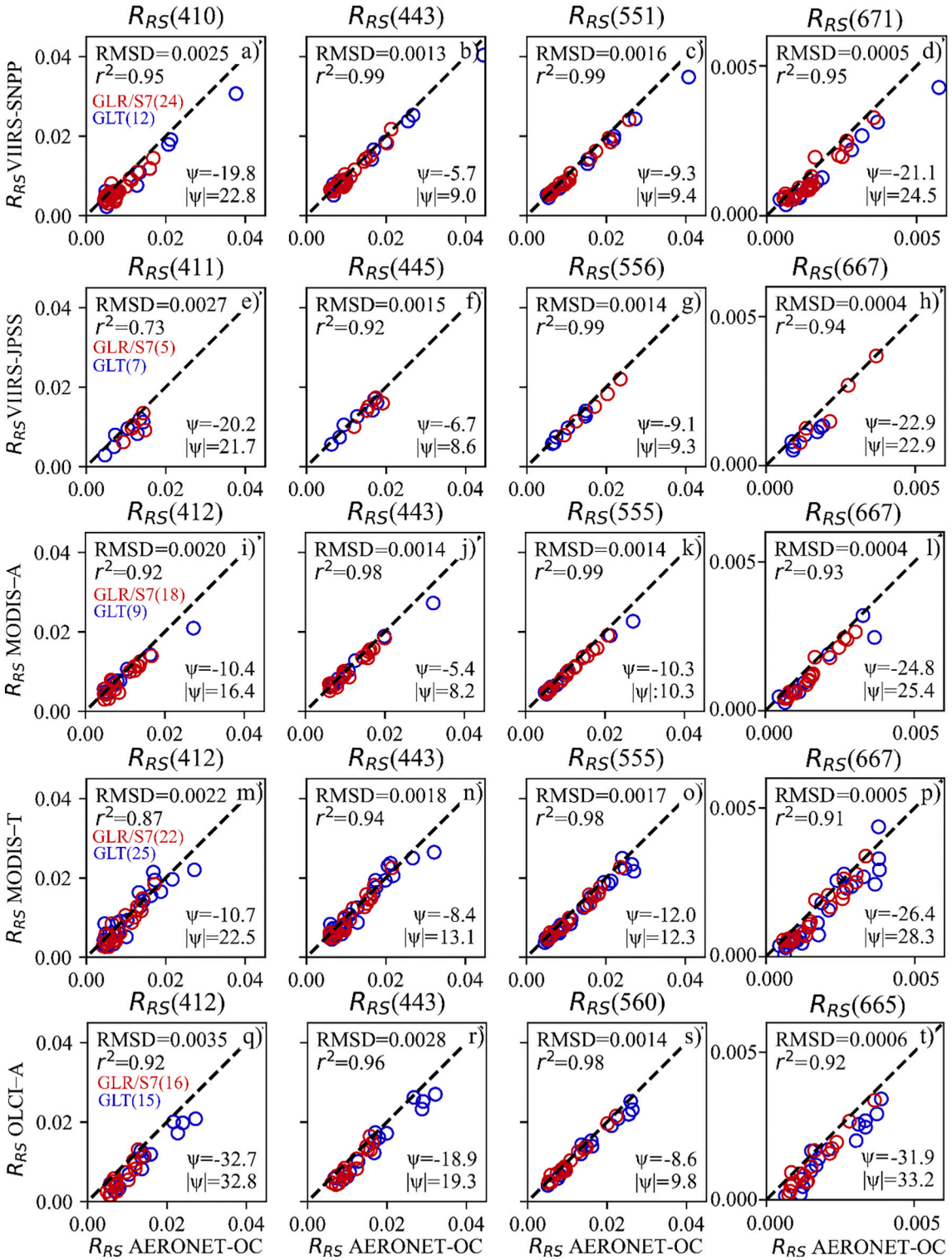

Fig. 5. Scatterplots summarizing matchup results for selected bands between AERONET-OC and satellite derived $R_{RS}(\lambda)$ in units of sr^{-1} for the Galata (GLT) and Gloria/Section-7 (GLR/S7) sites during the 2017 and 2020 coccolithophore bloom events. RMSD is in sr^{-1}, ψ (mean of relative differences) and $|\psi|$ (mean of absolute relative differences) are in %. The number of matchups is shown in brackets beside the site name in the first panel of each row.

by coccoliths for the major satellite ocean color missions. For each satellite sensor, Fig. 5 shows the scatterplots of $R_{RS}(\lambda)$ at selected center-wavelengths for matchups passing the filtering criteria and for which the AERONET-OC derived coccoliths flag is raised.

Notably, the number of matchups largely varies across missions regardless of the application of the same filtering criteria. This is mostly explained by differences in the acquisition frequency and swath width across missions. Then, for a given field datum, differences among data products from the various missions are the result of different calibration accuracies, radiometric performances, center-wavelengths, viewing geometries, and processing algorithms (i.e., from NASA or EUMETSAT).

Results indicate a determination coefficient r^2 usually above 0.9 and

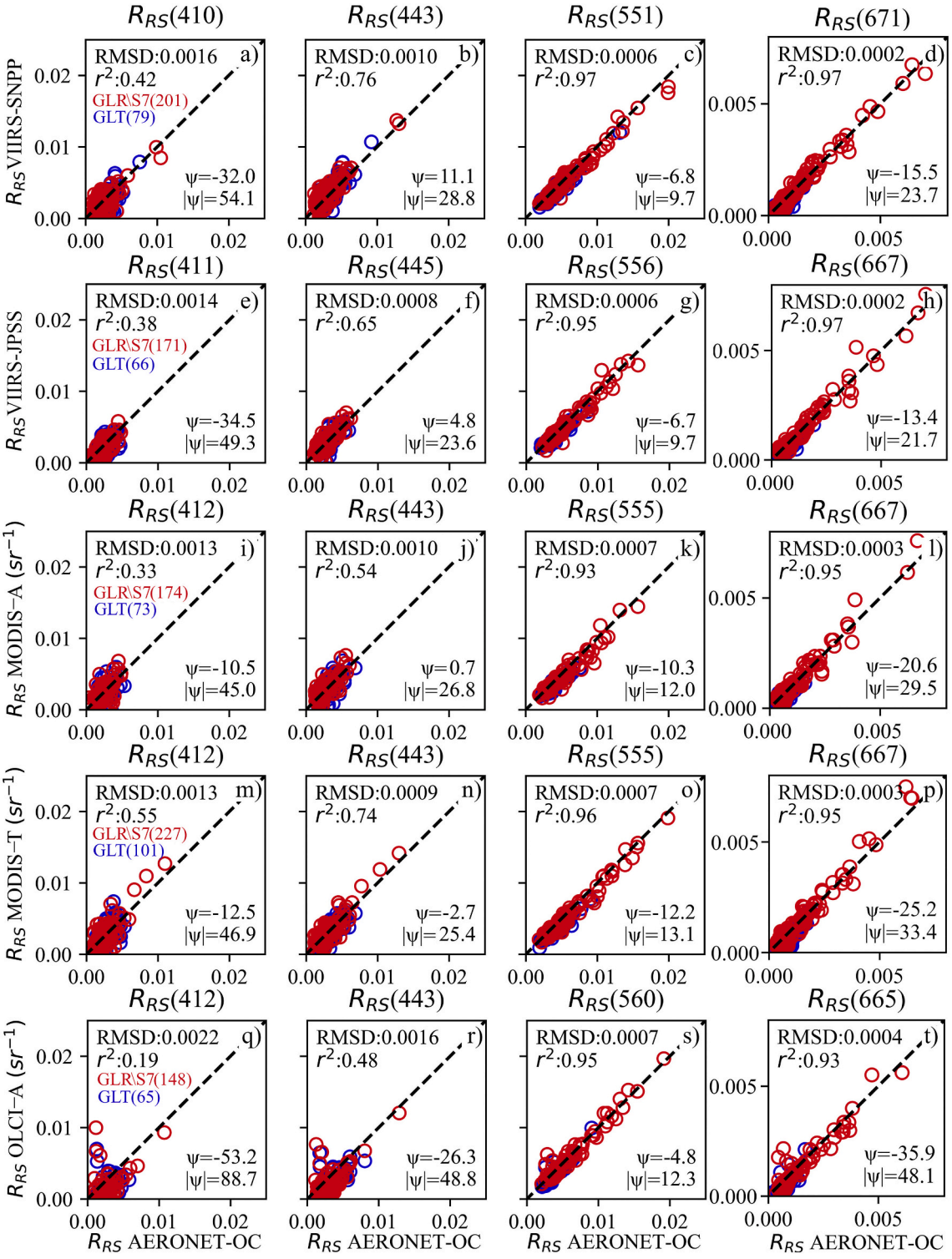

Fig. 6. Scatterplots summarizing matchup results for selected bands between AERONET-OC and satellite derived $R_{RS}(\lambda)$ in units of sr^{-1} for the Galata (GLT) and Gloria/Section-7 (GLR/S7) sites between 2018 and 2020, excluding data affected by coccoliths presence according to the coccoliths flag. RMSD is in sr^{-1}, ψ (mean of relative differences) and $|\psi|$ (mean of absolute relative differences) are in %. The number of matchups is shown in brackets beside the site name in the first panel of each row.

an overall underestimate of $R_{RS}(\lambda)$ across all sensors, more pronounced in the blue and red regions with ψ ranging between −33% for OLCI-A to −10% for MODIS-A in the blue and varying between −21% and −32% in the red. A general better performance is observed between 443 and 560 nm for all sensors, with an absolute minimum $\psi = -4.3\%$ at 469 nm (not shown in the scatterplots) for MODIS-A. Notably, in this spectral region, data generally show a much lower dispersion compared to the blue and red ones.

These results, even though relying on a relatively small number of matchups, appear consistent with those formally presented for MODIS-A and VIIRS-SNPP products for the Gloria site not accounting for the coccoliths flag (Zibordi et al., 2015). A complementary analysis, solely relying on matchups not affected by the coccoliths flag is presented in Fig. 6. Usually, differences are lower in the coccoliths cases when expressed in relative terms (ψ and $|\psi|$) and higher when expressed in units of sr^{-1} (RMSD), which is explained by the different ranges characterizing $R_{RS}(\lambda)$ in the two matchup datasets (i.e., the range is lower in the absence of coccoliths). For the same reason, r^2 is higher for the coccoliths matchup set. These results show that the $R_{RS}(\lambda)$ accuracy is not much degraded by the presence of coccoliths.

A good performance of the atmospheric correction should imply a correct determination of the radiance in the NIR spectral bands in the presence of coccolithophores, still recognizing it does not necessarily imply an equally accurate determination of the radiance at shorter center-wavelengths. In view of exploring such a feature of the atmospheric correction process in the NIR, AERONET-OC and satellite-derived $R_{RS}(\lambda)$ at 870 nm, or at corresponding center-wavelength, have been investigated. Specifically, Fig. 7 displays the $R_{RS}(870)$ time-series for the 2017 bloom event. Fig. 7a, referring to the Gloria site shows a notable agreement between in situ and all satellite derived $R_{RS}(870)$ during the entire bloom event (the random noise affecting the AERONET-OC data is due to the unavoidable uncertainties characterizing its spectrally asynchronous measurements (Zibordi et al., 2021)). On the contrary, Fig. 7b shows a good agreement between AERONET-OC and OLCI-A $R_{RS}(870)$, but increasing underestimates with the bloom evolution for MODIS and VIIRS. An explanation could be provided by a different performance of the two correction approaches in the presence of sediment-rich waters and coccolithophores. In fact, it is recalled that the Gloria region, opposite to Galata, is likely affected (as it was during the 2017 event) by the presence of estuarine waters. This may suggest a better capability of the EUMETSAT processor relying on the bright-pixel correction, to quantify non-negligible $R_{RS}(\lambda)$ in the sole presence of coccolithophores. Still, this better performance does not appear to lead to any superior determination of the radiometric products in the visible, where underestimates are large especially at the blue center-wavelengths.

The general underestimate of $R_{RS}(\lambda)$ affects the spectral $R_{RS}(\lambda)$ differences and thus *PIC* concentrations from the *CI*-based algorithm. Table 3 summarizes results obtained comparing *PIC* computed from AERONET-OC and satellite $R_{RS}(\lambda)$ with the absolute maximum ψ obtained for VIIRS-SNPP (i.e., −8.7%) and best performance obtained for MODIS-A (i.e., $\psi = -3.1\%$). It is recalled that these results do not refer to the uncertainties associated with the algorithm, but simply quantify how the algorithm outputs are affected by differences in $R_{RS}(\lambda)$.

3.4. Spectral evolution of $R_{RS}(\lambda)$ during coccolithophore blooms

The time-series of AERONET-OC in situ data at Galata and Gloria/Section-7 provide the unique opportunity for a comprehensive investigation of the spectral features of marine waters during the various phases characterizing coccolithophore blooms from their early growth through their decay.

Generally, for both events, AERONET-OC data show a rapid increase of $R_{RS}(\lambda)$ at comparable rates in the blue-green part of the spectrum at the beginning of the bloom. During this early phase, $R_{RS}(\lambda)$ in the green prevails over the blue values, which is likely due to the high absorption

Table 3
Matchup statistics for *PIC* values for each satellite sensor at both sites. The symbol ψ indicates the mean of relative differences, $|\psi|$ the mean of absolute relative differences (both expressed in %). RMSD indicates the root mean square of differences (in 10^{-3} mol m^{-3}), while the range is determined by the minimum and maximum values determined with AERONET-OC data (in 10^{-3} mol m^{-3}). *N* is the number of matchups.

VIIRS-SNPP ($N = 36$)	ψ	−8.7
	$\|\psi\|$	8.8
	RMSD	0.6
	Range (min-max)	2–16
VIIRS-JPSS ($N = 12$)	ψ	−8.5
	$\|\psi\|$	9.0
	RMSD	0.5
	Range (min-max)	2–9
MODIS-A ($N = 27$)	ψ	−3.1
	$\|\psi\|$	4.8
	RMSD	0.3
	Range (min-max)	2–11
MODIS-T ($N = 47$)	ψ	−4.7
	$\|\psi\|$	7.1
	RMSD	0.4
	Range (min-max)	1–11
OLCI-A ($N = 31$)	ψ	−8.1
	$\|\psi\|$	9.3
	RMSD	0.5
	Range (min-max)	2–11

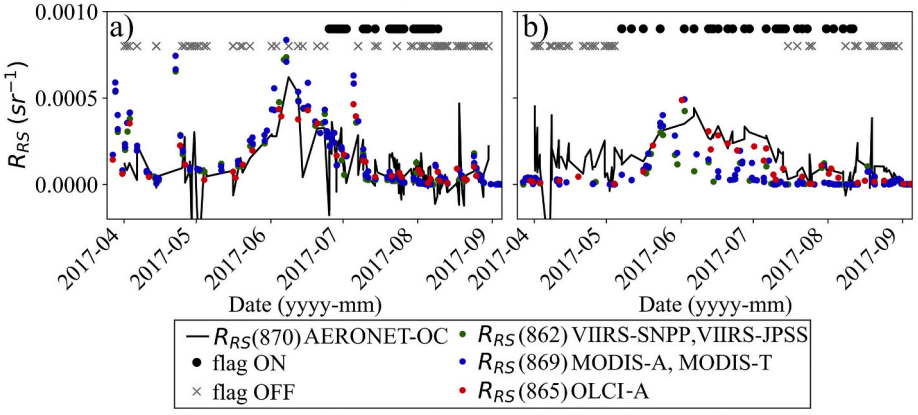

Fig. 7. Time series of AERONET-OC $R_{RS}(\lambda)$ at 870 nm from the (a) Gloria and (b) Galata sites for the 2017 coccolithophore event. The black • and grey × symbols indicate the values ON (raised) and OFF (not raised), respectively, of the coccoliths flag for each AERONET-OC measurement. The colored dots indicate satellite derived $R_{RS}(\lambda)$ at 870 nm (or at an equivalent center-wavelength) for MODIS-T, MODIS-A, VIIRS-JPSS, VIIRS-SNPP and OLCI-A.

by pigmented matter. On the contrary, the maximum of $R_{RS}(\lambda)$ spectra moves toward shorter wavelengths during the decaying phase of the bloom.

Figs. 8 through 11 show spectra of $R_{RS}(\lambda)$ during the blooms and their values normalized at 560 nm, $nR_{RS}(\lambda)$. The median and standard deviation from 2014 data are also shown as the background reference: these data are considered not affected by coccoliths and were determined for each site and yearly period spanning from May to July.

In detail, at the beginning of the bloom at Galata, the maximum value across the $R_{RS}(\lambda)$ spectra occurs between 490 and 530 nm (or 510 nm, depending on band availability). Panels a and c in Figs. 8 and 9 show that during this early phase, the $R_{RS}(\lambda)$ shape does not exhibit any dramatic change, but relatively higher values with respect to the $nR_{RS}(\lambda)$ reference spectrum, especially in 2017. $R_{RS}(\lambda)$ exhibits a maximum at 490 or 510 nm in 2020, and alternatively at 490 or 532 nm in 2017, with $R_{RS}(443)$ lower than $R_{RS}(551)$ or $R_{RS}(560)$. At the bloom peaks identified by the *PIC* maxima, $R_{RS}(\lambda)$ spectra exhibit their highest values at 490 nm, exceeding 0.05 sr^{-1} on June 6th 2017 and approaching 0.03 sr^{-1} on May 25th 2020 (while the median value is lower than 0.005 sr^{-1} in the absence of coccoliths). After the bloom peaks (see panels b and d in Figs. 8 and 9) with the coccoliths scattering prevailing in the blue, $R_{RS}(\lambda)$ values in the green spectral region decrease more rapidly than in the blue with $R_{RS}(443)$ prevailing over $R_{RS}(551)$ and $R_{RS}(560)$, while $R_{RS}(510)$ or alternatively $R_{RS}(530)$ is always lower than $R_{RS}(490)$.

At Gloria/Section-7, a spectral dependence similar to that characterizing the Galata data is confirmed at the beginning of the 2020 bloom, despite a complex temporal evolution likely explained by the effects of the Danube waters and local dynamics. This evolution, however, is very different from that observed during the 2017 event (see Fig. 10). In fact, the $R_{RS}(\lambda)$ values of 2017, in the initial phase of the bloom, show their highest values alternatively at 530 or 551 nm, with $R_{RS}(\lambda)$ and $nR_{RS}(\lambda)$ spectra comparable to the reference spectrum. Again, the impact of the Danube waters likely lessens the signature of the bloom and may also affect the performance of the coccoliths flag, which was proposed for a different type of waters. In fact, for the 2017 event at Gloria the coccoliths flag is only effective after the peak date tentatively corresponding to the maximum *PIC* value. Nonetheless, the estimated *PIC* already increases, with a value exceeding 10×10^{-3} mol m^{-3} on June 8th 2017. Only at the end of June the coccoliths flag is raised and the $R_{RS}(\lambda)$ spectra exhibit maxima shifted toward the blue center-wavelengths with $R_{RS}(443)$ prevailing over $R_{RS}(551)$.

During the initial phase of the bloom in 2020, the $R_{RS}(\lambda)$ spectra show a plateau between 490 and 560 nm (see panels a and c in Fig. 11), with much higher normalized values at shorter wavelengths with respect to the reference spectrum. When compared to the $R_{RS}(\lambda)$ spectra from Galata for the same period, the slope in the green is less pronounced until the occurrence of the first peak of the bloom. After that, $R_{RS}(490)$ prevails until the end of the bloom, even in correspondence of lower *PIC* values. In this case too, $R_{RS}(443)$ is usually higher than $R_{RS}(560)$ during the decline of the bloom.

It is noted that at the bloom peak, the computed *PIC* values are generally higher at Galata than at Gloria in 2017 (Figs. 8 and 10 show peak values of 15.9×10^{-3} versus 10.1×10^{-3} mol m^{-3}), while the opposite occurs in 2020 (Figs. 9 and 11 show peak values of 8.3×10^{-3} versus 11.5×10^{-3} mol m^{-3}) as also shown by the *CI* values proportional to *PIC* displayed in Figs. 12 and 13.

It is expected that the $R_{RS}(\lambda)$ relative spectral changes observed during coccolithophore blooms have an effect on the band ratios *R1*, *R2* and *R3* applied to set the coccoliths flag. Figs. 12 and 13 display the values of *R1*, *R2* and *R3* during each bloom as a function of time in conjunction with the *CI* difference applied for computing *PIC*, which qualitatively indicates the bloom progression for both AERONET-OC and satellite data. However, the different band setting for each sensor and AERONET-OC deployment causes differences in the *R2* and *R3* values. For this reason, only MODIS-A and MODIS-T results are shown in Fig. 12c and d, and only VIIRS-SNPP and VIIRS-JPSS ones in Fig. 13. This choice was suggested by the higher temporal resolution of these products and center-wavelengths better corresponding to those of the AERONET-OC data applied for the computation of band ratios (see Sections 2.1 and 4 for band settings). Daily means and standard deviations are displayed for both AERONET-OC and satellite data (for the latter, when data from multiple sensors are available for the same date,

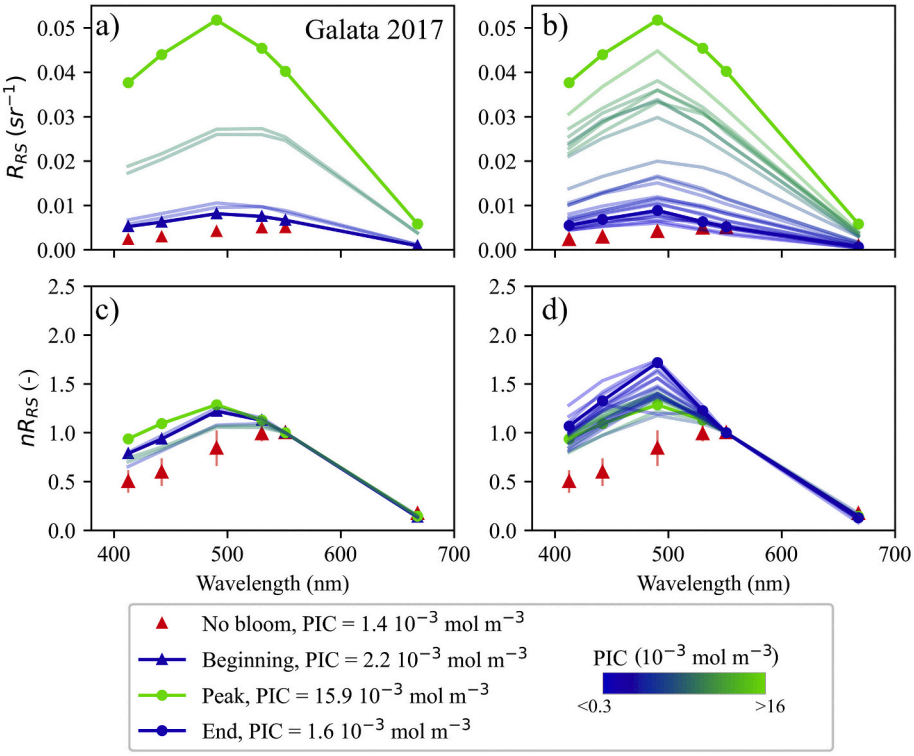

Fig. 8. Daily median AERONET-OC $R_{RS}(\lambda)$ spectra (a, b) and their normalized values $nR_{RS}(\lambda)$ at 551 nm (c, d) during the 2017 bloom event at Galata. Panels a and c refer to data acquired up to the bloom peak while panels b and d refer to the data acquired after the peak. Colors indicate the *PIC* values, also provided for selected dates: May 7th (in the bloom initial phase), June 6th (corresponding to the bloom peak), August 10th (during the bloom decay). The median and standard deviation calculated from 2014 data are indicated in red. (For interpretation of the references to color in this figure legend, the reader is referred to the web version of this article.)

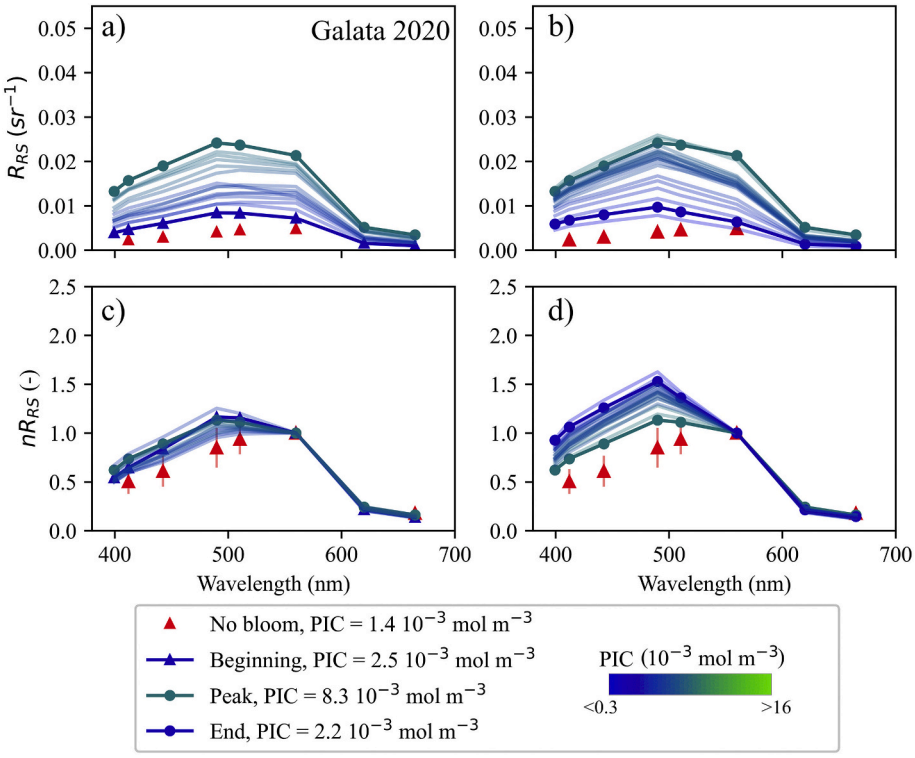

Fig. 9. Daily median AERONET-OC $R_{RS}(\lambda)$ spectra (a, b) and their normalized values $nR_{RS}(\lambda)$ at 560 nm (c, d) during the 2020 bloom event at Galata. Panels a and c refer to data acquired up to the bloom peak while panels b and d refer to data acquired after the peak. Colors indicate the *PIC* values, also provided for selected dates: May 2nd (in the bloom initial phase), May 25th (corresponding to the bloom peak), June 22nd (during the bloom decay). The median and standard deviation calculated from 2014 data are indicated in red. (For interpretation of the references to color in this figure legend, the reader is referred to the web version of this article.)

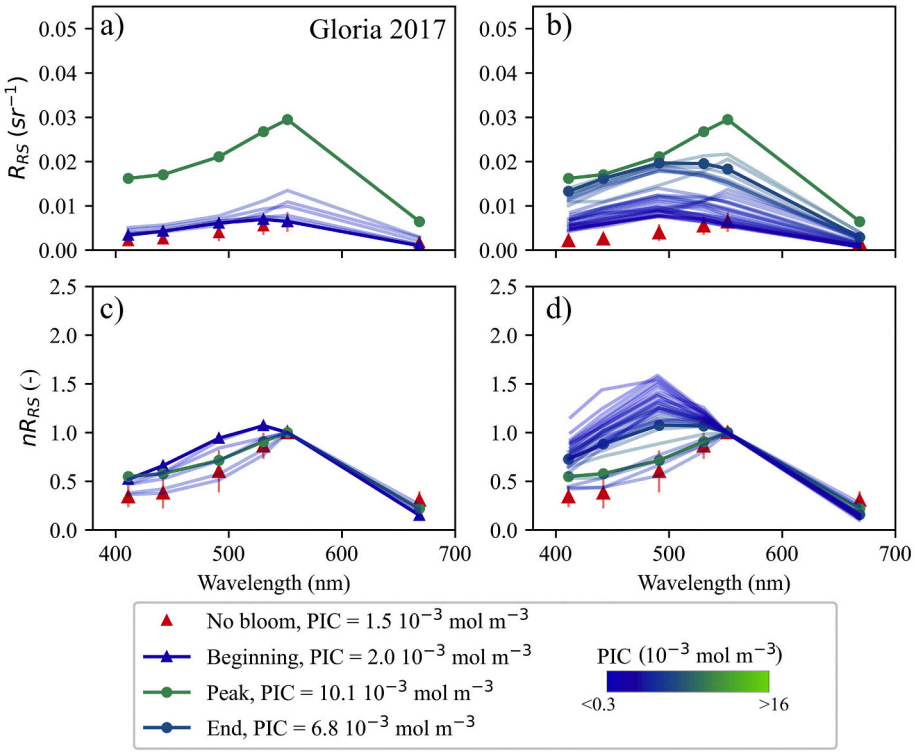

Fig. 10. Daily median AERONET-OC $R_{RS}(\lambda)$ spectra (a,b) and their normalized values $nR_{RS}(\lambda)$ at 551 nm (c,d) during the 2017 bloom event at Gloria. Panels a and c refer to data acquired up to the bloom peak while panels b and d refer to data acquired after the peak. Colors indicate the *PIC* values, also provided for selected dates: May 16th (in the bloom initial phase), June 8th (corresponding to the bloom peak), June 26th (during the bloom decay). The median and standard deviation calculated from 2014 data are indicated in red. (For interpretation of the references to color in this figure legend, the reader is referred to the web version of this article.)

their mean and standard deviation are shown). The band ratio values for data exhibiting the coccoliths flag raised are displayed with solid circles, and are the sole applied to determine the linear regressions. For completeness, the values exhibiting the coccoliths flag 'OFF' are displayed as empty circles.

As expected from the spectral analysis of $R_{RS}(\lambda)$ with the coccoliths flag raised during the different phases of the blooms, the ratios show a clear temporal trend with a general increase for both field and satellite data. Considering the AERONET-OC data, *R1*, *R2* and *R3* show the fastest increase for *R1*, at both sites, with the highest values in 2020. The angular coefficient resulting from a robust linear regression for *R1*, *R2*, *R3* are 0.0036, 0.0011, 0.0022 day^{-1} and 0.0040, 0.0021, 0.0018 day^{-1}

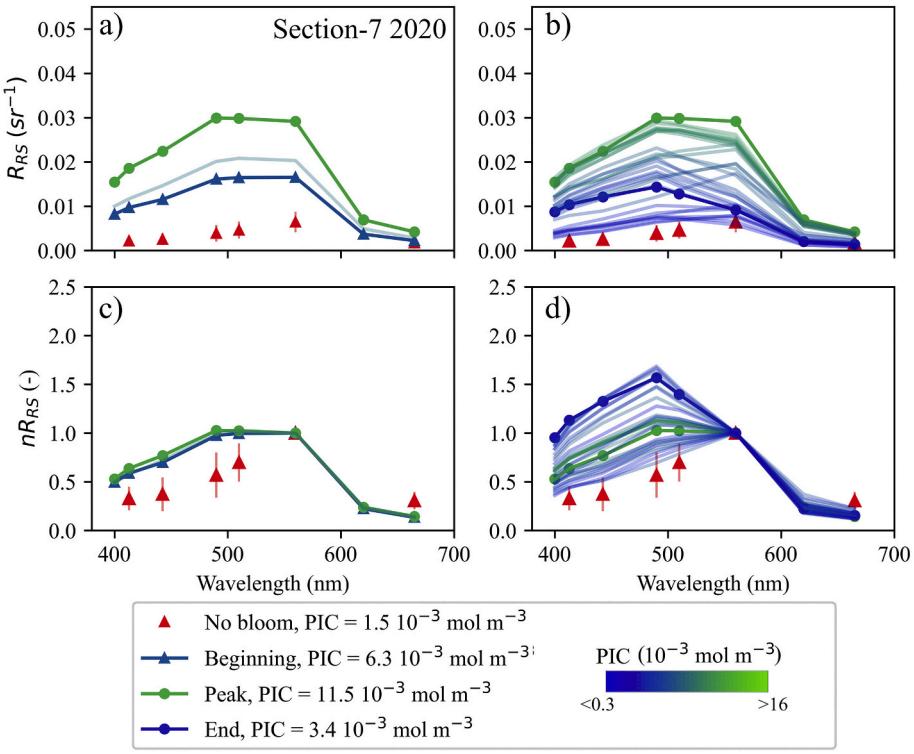

Fig. 11. Daily median AERONET-OC $R_{RS}(\lambda)$ spectra (a,b) and their normalized values $nR_{RS}(\lambda)$ at 560 nm (c,d) during the 2020 bloom event at Section-7. Panels a and c refer to data acquired up to the bloom peak while panels b and d refer to data acquired after the peak. Colors indicate the *PIC* values, also provided for selected dates: May 10th (in the bloom initial phase), May 17th (corresponding to the *PIC* peak), June 28th (during the bloom decay). The median and standard deviation calculated from 2014 data are indicated in red. (For interpretation of the references to color in this figure legend, the reader is referred to the web version of this article.)

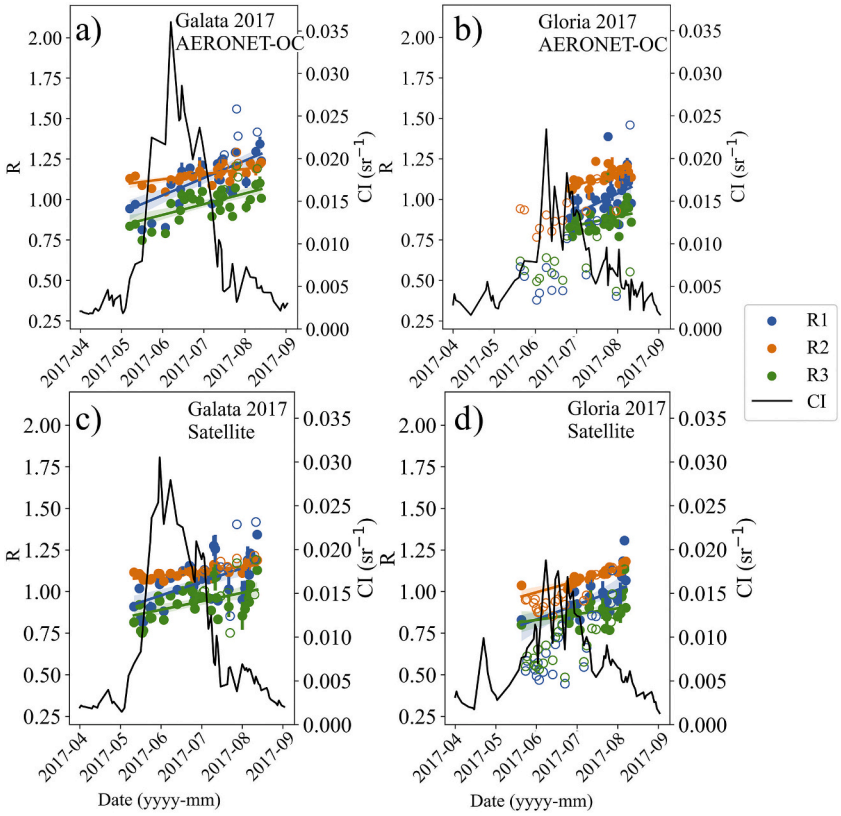

Fig. 12. Band ratio *R* (i.e., *R1*, *R2*, *R3*) and *CI* mean daily values and standard deviations for the 2017 coccolithophore bloom, determined from Galata (a,c) and Gloria (b,d) AERONET-OC data (a,b), and from MODIS-T and MODIS-A products (c,d). Values from multiple sensor data were averaged for each day. The result of a robust linear regression with relative confidence interval at 95% (displayed through shaded areas) is also shown for each series of band ratio values (limited to cases with the coccoliths flag raised). Filled and empty circles indicate *R1*, *R2* and *R3* ratio values for dates when the coccoliths flag is and is not activated, respectively. In panel b, AERONET-OC values are also shown before the first activation to provide a coherent time-series with the satellite one.

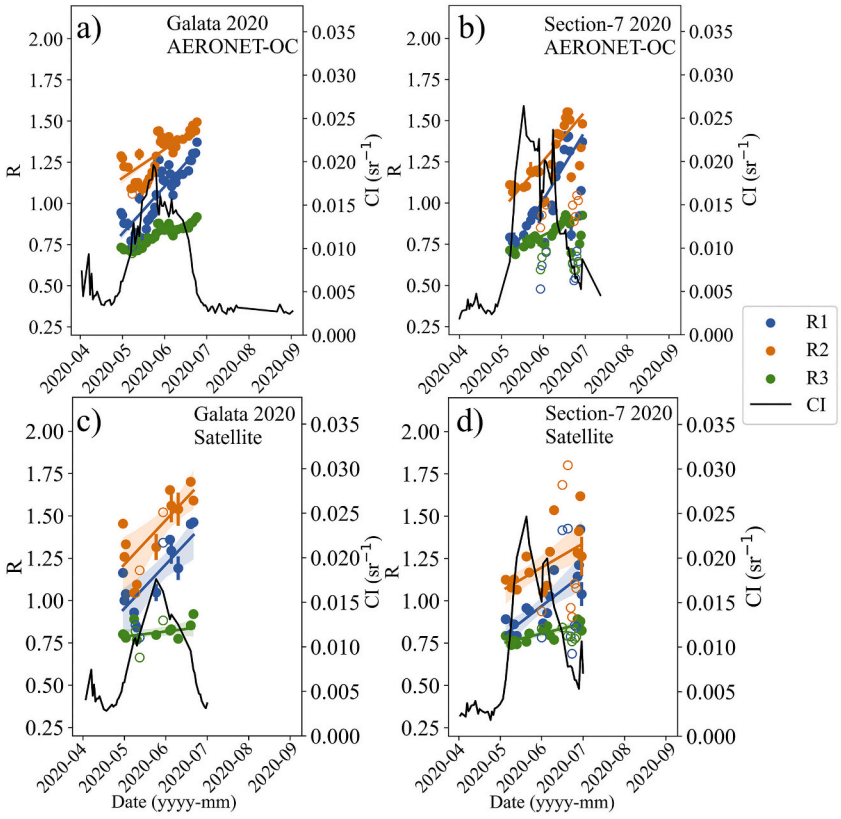

Fig. 13. Band ratio *R* (i.e., *R1*, *R2*, *R3*) and *CI* mean daily values and standard deviations for the 2020 coccolithophore bloom, determined from Galata (a,c) and Section-7 (b,d) AERONET-OC data (a,b), and from VIIRS-JPSS and VIIRS-SNPP products (c,d). Values from multiple sensor data were averaged for each day. The result of a robust linear regression with relative confidence interval at 95% (displayed through shaded areas) is also shown for each series of band ratio values (limited to cases with the coccoliths flag raised). Filled and empty circles indicate *R1*, *R2* and *R3* ratio values for dates when the coccoliths flag is and is not activated, respectively.

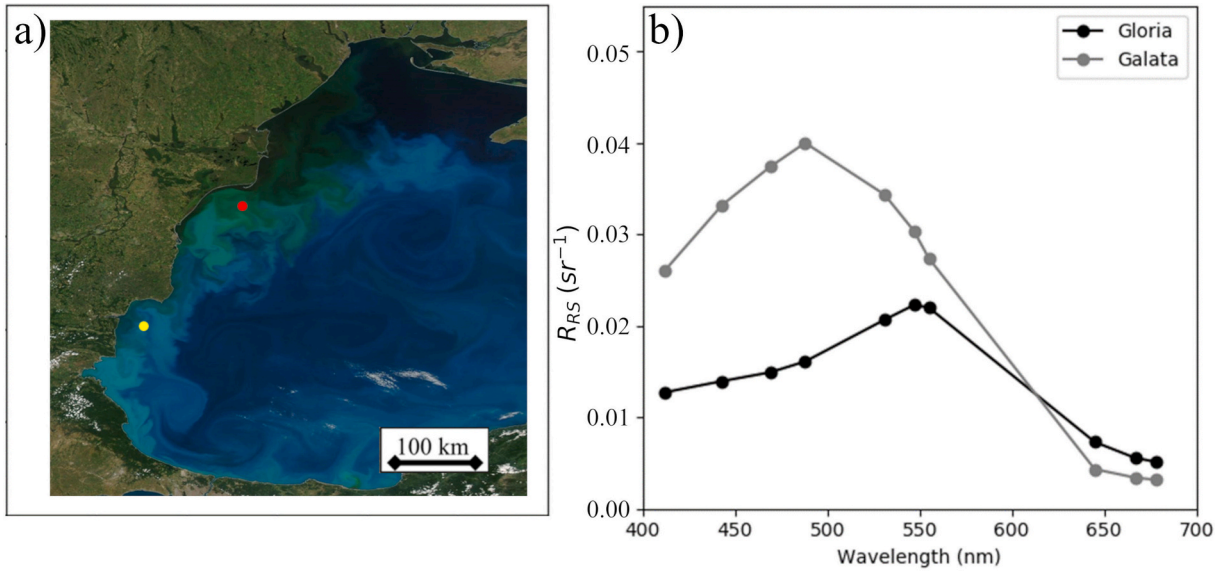

Fig. 14. Coccolithophore bloom on June 7th 2017: (a) True color MODIS-A image over study area generated through EOSDIS worldview with corrected reflectance products using the MODIS bands 1, 4 and 3 for the red, green and blue, respectively (see https://earthdata.nasa.gov/faq/worldview-snapshots-faq#modis-true-color for product description). Dots indicate the Gloria/Section-7 and Galata sites in red and yellow, respectively. (b) MODIS-T $R_{RS}(\lambda)$ on June 7th 2017 at the Galata and Gloria sites. (For interpretation of the references to color in this figure legend, the reader is referred to the web version of this article.)

in 2017, and 0.0095, 0.0058, 0.0037 day^{-1} and 0.0135, 0.0096, 0.0041 day^{-1} in 2020, at Galata and Gloria/Section-7, respectively. When comparing these values, it should be taken into account that different band settings were available in the two different years, and consequently *R2* and *R3* were calculated using $L_{WN}(530)$ in 2017 and $L_{WN}(510)$ in 2020.

4. Discussion

The analysis of the evolution of the spectral shape of $R_{RS}(\lambda)$ data during the 2017 and 2020 Black Sea coccolithophore blooms highlights a larger variation with time at the blue with respect to the green center-wavelengths. Groom and Holligan (1987) already documented that the

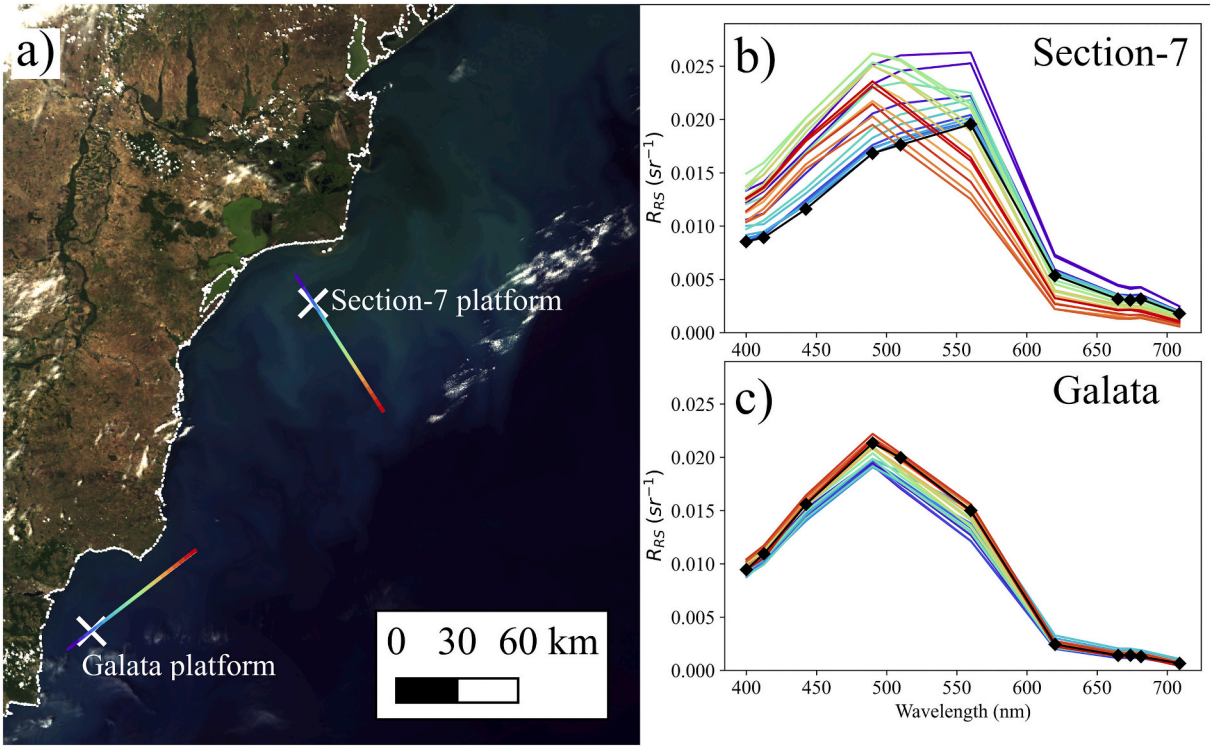

Fig. 15. (a) OLCI-A True Color image of the Western Black Sea, generated applying the S3 toolbox to Level-1 Full Resolution products of 2020 May 31st, using the bands 8, 6 and 4 for the red, green and blue, respectively. The plots show the $R_{RS}(\lambda)$ spectra along transects crossing Section-7 (b) and Galata (c) from the corresponding OLCI-A Level-2 Full Resolution products. The spectra corresponding to the AERONET-OC locations are displayed in black. (For interpretation of the references to color in this figure legend, the reader is referred to the web version of this article.)

blue reflectance relative to the green one usually tends to be low at the beginning of a bloom because of a higher pigment concentration or cell-to-coccoliths ratio. This explanation was recently confirmed by radiative transfer simulations (Neukermans and Fournier, 2018). Those results showed that, while during the initial stage of the bloom the absorption from the coccolithophores cores impacts the $R_{RS}(\lambda)$ magnitude and shape by reducing the reflectance in the blue, during the decaying phase the $R_{RS}(\lambda)$ maximum shifts toward the blue-turquoise wavelengths as a result of cores death and accumulation of detached coccoliths. These theoretical findings are experimentally consolidated in this study through results from the analysis of in situ and satellite derived $R_{RS}(\lambda)$.

However, as expected, results also indicate that $R_{RS}(\lambda)$ variations and the activation of the coccoliths flag can be impacted by local perturbations not related to the bloom phenology. In this respect, the optically complex waters of the Danube plume may strongly affect the radiometric signal at the Gloria/Section-7 location, likely explaining the short-term abrupt changes in $R_{RS}(\lambda)$ displayed in panels c and d of Fig. 2 (as illustrated in Fig. 3). This is clearly shown by a reduction of $R_{RS}(\lambda)$ in the marine regions affected by the Danube waters at the beginning of the 2017 bloom and toward the end of the 2020 one. Figs. 14 and 15 display two examples produced from MODIS-A and OLCI-A imagery. Fig. 14a shows that, on June 7th 2017 (i.e., at the bloom peak), the coccoliths presence at Gloria, in comparison to Galata, is marked by more brownish waters leading to a MODIS $R_{RS}(\lambda)$ spectrum exhibiting maximum at around 560 nm with values decreasing toward the blue (see panel b in Fig. 14). Fig. 15, instead, shows the spatial variability through OLCI-A $R_{RS}(\lambda)$ spectra along two transects: one crossing Section-7, the Danube plume and the nearby region clearly characterized by the coccolithophore bloom; and the other one intersecting Galata and the nearby bloom region. The $R_{RS}(\lambda)$ spectra away from the coast along the Gloria/Section-7 transect are similar to the spectra along the Galata one, with features typical of water optical properties affected by the presence of coccoliths. Conversely, the $R_{RS}(\lambda)$ spectra closer to the Danube mouth show values relatively higher in the green and, in some cases lower at 412 nm, which suggests the presence of detritus particles and dissolved substances associated with the Danube waters.

In order to consolidate these conclusions, bloom evolutions were also investigated in regions of: *i.* the Central Black Sea away from the coast and consequently expected to be less affected by estuarine waters; and *ii.* the Celtic Sea and the North Sea characterized by water types different from those typical of the Black Sea. For each case, the $R_{RS}(\lambda)$ values were determined from 3 × 3 image elements extracted from MODIS-A and MODIS-T data products. The related *PIC* and band ratio values were determined in agreement with the methodology detailed in Section 2.2.

With reference to the Black Sea 2017 event, the offshore $R_{RS}(\lambda)$ usually show the highest values at 469 or 488 nm with $R_{RS}(\lambda)$ increasing faster at 443 and 488 nm than at longer center-wavelengths in the proximity of the peak date. Notably, the coccoliths flag is raised more rarely than at the AERONET-OC sites: in some case it is raised occasionally, in some other only at the late stage of the bloom when *CI* already exhibits low values. This could be explained by very high values of *R3* (calculated with $L_{WN}(443)$ and $L_{WN}(531)$ for MODIS) not meeting the threshold defined to raise the coccoliths flag as a result of biases in satellite-derived $R_{RS}(\lambda)$ affecting the performance of the flag, or also relatively low concentrations of coccoliths.

An alternative to the coccoliths flag is *CI* appearing more effective in identifying turquoise waters. Still, the assessment of the performance of either the coccolith flag or *CI*, would require in situ measurements of coccolithophores concentrations, which are not available for this study.

Fig. 16 shows the $R_{RS}(\lambda)$ evolution for a location in the Central Black Sea (43.32°N, 32.27°E, see Fig. 4) chosen because the related *PIC* concentrations are comparable to those observed at the AERONET-OC sites. With respect to the reference spectrum (referring to pre-bloom conditions at the location), $R_{RS}(\lambda)$ exhibits values increasing up to approximately 15 times at 490 nm during the bloom growth (see panel a and b) while preserving a similar shape (see the $nR_{RS}(\lambda)$ values in panel c).

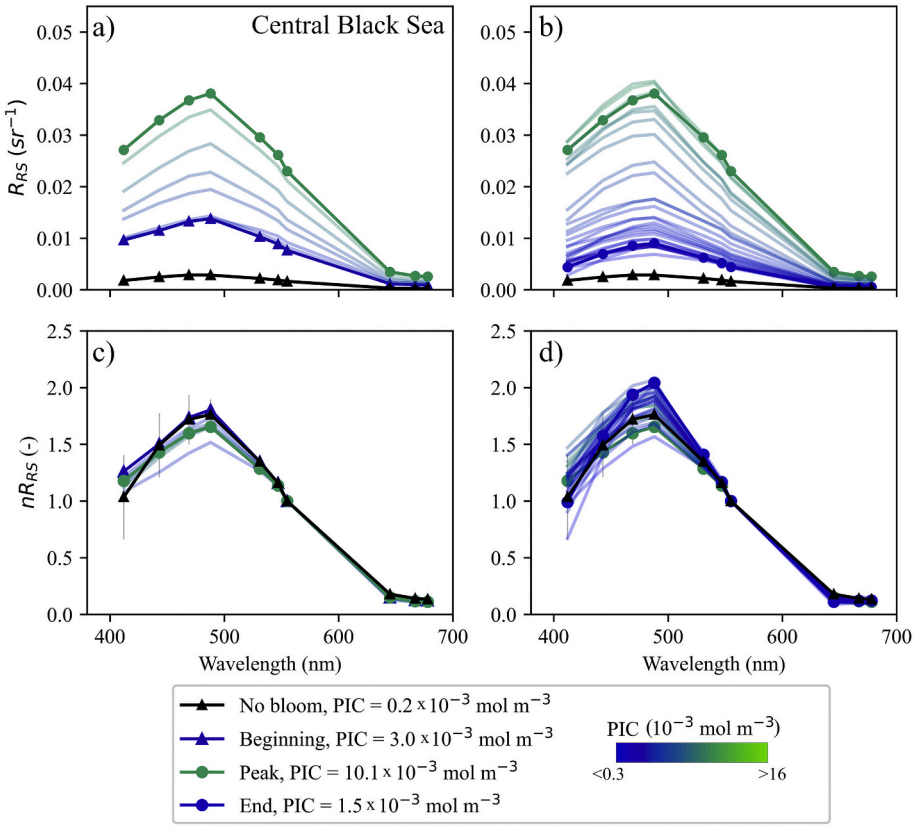

Fig. 16. MODIS-A and MODIS-T $R_{RS}(\lambda)$ spectra (a,b) and their normalized values $nR_{RS}(\lambda)$ at 555 nm (c,d) during the 2017 bloom event at a location in the Central Black Sea. Panels a and c refer to data acquired up to the bloom peak while panels b and d refer to data acquired after the peak. Colors indicate the *PIC* values, also provided for selected dates: May 28th (during the initial phase of the bloom), June 21st (corresponding to the bloom peak), August 7th (during the bloom decay). When multiple satellite products are available for the same date, the mean spectrum is shown. As a reference, the median and standard deviation values calculated over April 2017, before the bloom starts, are indicated in black in each panel.

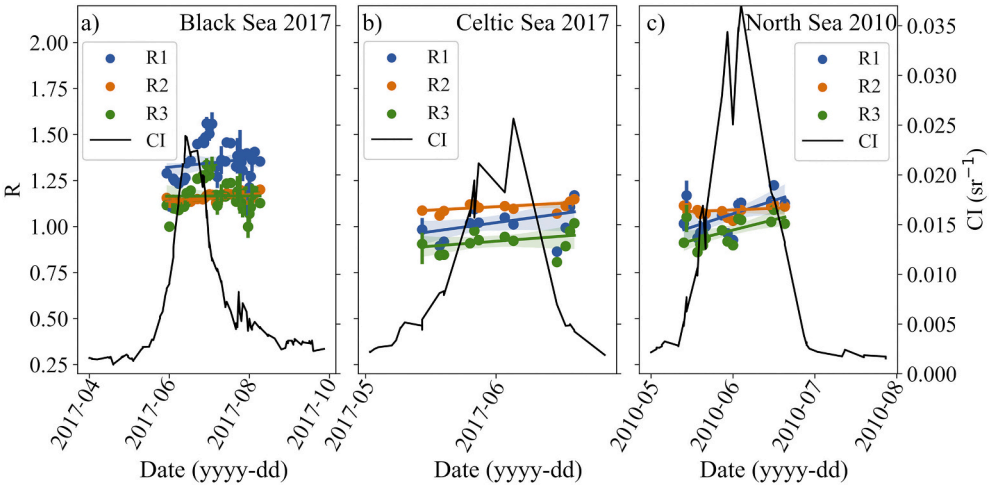

Fig. 17. Band ratio *R* (i.e., *R1*, *R2*, *R3*, mean daily values and related standard deviation) and *CI* values from MODIS-T and MODIS-A derived products for the coccolithophore blooms in the Central Black Sea in 2017 (a), in the Celtic Sea in 2017 (b) and in the North Sea in 2010 (c). The result of a robust linear regression and relative confidence interval at 95% (displayed through shaded areas) for each band ratio series is also shown. All points in the identified period are displayed, regardless of the coccoliths flag activation.

Conversely, during the decaying phase $nR_{RS}(\lambda)$ shows a more pronounced value in the blue spectral region (see panel d).

Fig. 17a shows the band ratios *R1*, *R2* and *R3* for the Central Black Sea location during the bloom as identified by the coccoliths flag, for all points within the first and last activation. The band ratios notably increase in the period around the bloom peak (about 1 week before and 3 weeks after the *PIC* maximum). However, on July 5th 2017 the $R_{RS}(\lambda)$ values in the 443–490 nm spectral region decrease suddenly, leading to a drop in the ratios, which later increase again up to the end of the bloom. From the examination of other locations away from the coastal regions, the increase in ratios with time does not appear to be a general feature when considering MODIS data.

Panels b and c in Fig. 17 refer to coccolithophore bloom events identified in the Celtic Sea (51.26°N, 5.8°W) in 2017 and in the North Sea (56.33°N, 6.30°E) in 2010, respectively (see Fig. 18). With reference to the Celtic Sea event, the cloud cover prevented observing the entire evolution of the bloom. Still for some location, data show increasing values of *R1*, *R2* and *R3* from the first to last occurrence of activated coccoliths flags although a robust linear regression is only evident for *R2*. More marked is the positive and robust trend shown by *R1* and *R3* for the North Sea event. Still, *R2* does not exhibit any trend. It is worth recalling that *R2* for MODIS data is computed with $R_{RS}(531)$. The same spectral band was used for *R2* calculated with 2017 AERONET-OC data which showed modest trends (see Section 3.4) at the two sites. Conversely, the use of $R_{RS}(510)$ in *R2* led to more pronounced trends in the AERONET-OC series from 2020. These results suggest that

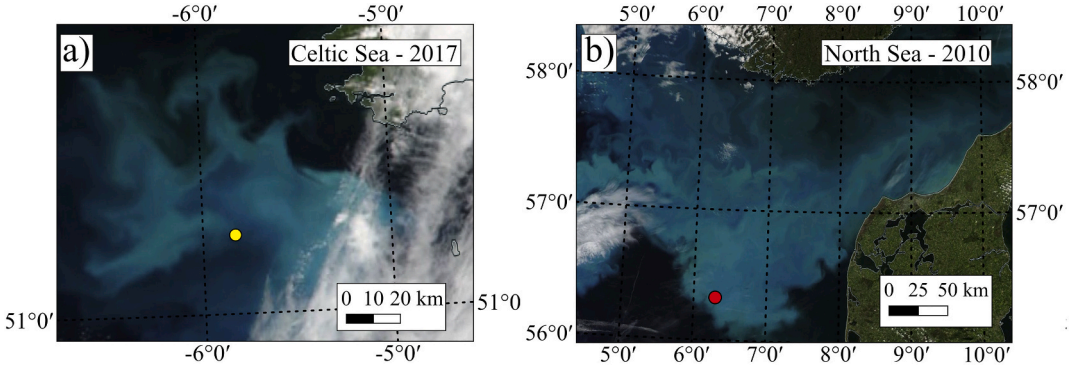

Fig. 18. True color VIIRS-SNPP imagery showing the coccolithophores bloom in (a) the Celtic Sea on June 2nd 2017 and (b) in the North Sea on June 3rd 2010. The true color images were downloaded from EOSDIS worldview with corrected reflectance products using the VIIRS-SNPP bands I1, M4 and M3 for the red, green and blue, respectively (see https://earthdata.nasa.gov/faq/worldview-snapshots-faq#snpp-true-color for products description). Yellow and red dots indicate the points related to the time series in Fig. 17. (For interpretation of the references to color in this figure legend, the reader is referred to the web version of this article.)

Table 4
Confusion matrix showing the activation of the coccoliths flag for the matchup data across the entire AERONET-OC time-series at Galata and Gloria/Section-7 sites since 2014. Values are expressed in percentage with respect to the number of matchups indicated in brackets below the sensor name.

		VIIRS-SNPP (549)		VIIRS-JPSS (274)		MODIS-A (521)		MODIS-T (706)		OLCI-A (336)	
		ON	OFF	ON	OFF	ON	OFF	ON	OFF	ON	OFF
AERONET-OC	ON	7	2	4	3	6	2	6	4	8	6
	OFF	1	90	<1	93	<1	92	<1	89	<1	86

wavelengths around 530 nm are in general too close to the green to reveal a clear trend in the *R2* ratio.

Building on previous considerations on the performance of the coccoliths flag in relation to the sensor band settings, it is reminded that the matchups analyzed in this study rely on flag values solely determined with AERONET-OC $L_{WN}(\lambda)$ data. This choice has ensured independence of results from different center-wavelengths (i.e., 445, 489, 556 nm for VIIRS-JPSS; 443, 486, 551 nm for VIIRS-SNPP; and 443, 531, 547 nm for MODIS-A and MODIS-T; 443, 510, 560 nm for OLCI-A). It is thus of interest to explore the capability of data products from different missions to correctly detect coccoliths, keeping in mind that the lack of in situ data on coccoliths concentration only allows verifying the consistency between AERONET-OC and satellite derived values of the coccoliths flag.

Table 4 shows the confusion matrix produced for various satellite data products at the AERONET-OC sites using all available matchups. For each matchup, the flag was set 'ON' for AERONET-OC data if it was activated for at least one measurement in a 2-h time window from the satellite overpass. Conversely, for satellite data it was activated when at least 50% of the 3 × 3 elements considered for the analysis had the coccoliths flag raised. Results show the consistency of MODIS and VIIRS flagging for coccoliths, with almost no false positive but with some false negative (from 2 to 3% for VIIRS and from 2 to 4% for MODIS, still representing a large fraction of those identified as positive through AERONET-OC data). Even though some disagreement (false positive or negative) happens at the scale of the single day and location, the overall agreement (sum of diagonal terms) for MODIS and VIIRS products varies from 95% to 98% and suggests that the various satellite missions have potentials to support investigations on the evolution of a bloom in the region (as anticipated by Table 2). Also, results obtained applying the NASA coccoliths flag algorithm to OLCI-A show fair consistency with other missions.

5. Conclusions

The spectral signature of major coccolithophore blooms occurring in the Black Sea in 2017 and 2020 were investigated using $R_{RS}(\lambda)$ from two AERONET-OC sites and various satellite ocean color missions. This invaluable time-series of reference measurements allowed to investigate the coccolithophore blooms at distinct locations diversely affected by the Danube waters by documenting the spectral, temporal and spatial variability of marine waters during these events. In particular, it allowed assessing the spectral changes of $R_{RS}(\lambda)$ during blooms in the study area, which is relevant to evaluate algorithms applied for coccoliths detection, and to identify successive stages of bloom evolution that could be put in relation with different levels of cells-to-liths ratios. The in situ data also permitted the assessment of satellite derived $R_{RS}(\lambda)$ over marine regions characterized by coccolithophore blooms and extremely high scattering properties.

By investigating the blooms evolution from the radiometric point of view, at both temporal and spatial scale, the study led to the following findings:

a. An expected increase of $R_{RS}(\lambda)$ was observed during the coccolithophore events, more pronounced in the blue-green spectral region, with peaks occurring between 490 nm and 530 nm at Galata and between 490 nm and 560 nm at Gloria/Section-7. $R_{RS}(\lambda)$ were extremely high during the 2017 event with $R_{RS}(490)$ exceeding 0.05 sr^{-1}, i.e., 10 times the median value characterizing the region in the absence of coccoliths.
b. A shift in the $R_{RS}(\lambda)$ spectral shape characterized the blooms evolution at the AERONET-OC sites. In particular, when the blooms approached their peak, the intensity of $R_{RS}(\lambda)$ in the blue prevailed over the one in the green as a result of the accumulation of detached coccoliths and the death of absorbing cell cores. A similar dependence, although less pronounced, was observed during coccolithophore blooms from the analysis of satellite derived $R_{RS}(\lambda)$ in some regions in the Central Black Sea, Celtic Sea and North Sea. It is however acknowledged that this behavior is not systematic because the spectral variations are impacted by the background optical properties of sea water. It is also recognized that an analysis conducted at a fixed location is prone to being influenced by local dynamics that may affect the spatial homogeneity of coccoliths concentration and optical properties of sea water.

c. Differences between coccolithophore bloom evolutions observed at the AERONET-OC sites were largely explained by the impact of the Danube estuarine waters. This was particularly evident for the Gloria/Section-7 location, where data showed the occurrence of relative minima alternated to maxima in $R_{RS}(\lambda)$ time-series, or the existence of extremely high $R_{RS}(\lambda)$ in the green spectral region at the late stage of blooms, suggesting the presence of high concentrations of suspended particles.
d. The application of the NASA coccoliths flag, proposed for oceanic waters, is naturally affected by the presence of high concentrations of colored dissolved organic matter and detritus particles, and its values might not always match the evolution of *PIC* as estimated by the *CI*-based algorithm. Still, with some caution, it remains a valuable tool for coccolithophore bloom investigations in the Black Sea optically complex waters.

Satellite derived $R_{RS}(\lambda)$ analysis showed that:

e. Overall, $R_{RS}(\lambda)$ satellite data products from the main ocean color missions do not exhibit a significantly degraded accuracy for observations performed in conditions characterized by the presence of coccoliths. Still, all satellite data products show a generic underestimate of the $R_{RS}(\lambda)$ values.
f. Satellite derived $R_{RS}(\lambda)$ show consistency with the AERONET-OC derived spectral evolutions of coccolithophore bloom events. However, the activation of the coccoliths flag determining the presence of coccoliths may sometime exhibit false negative cases when applied to satellite data with respect to AERONET-OC data. This is naturally explained by the use of center-wavelengths not exactly matching those for which the coccoliths flag was proposed and by biases affecting satellite-derived $R_{RS}(\lambda)$. On coccoliths identification, *CI* appears more effective. Still, any application relying on it would require measurements of coccolithophores concentrations, which are not available for this study.
g. The algorithm applied in the study exhibits underestimates ranging between -3.1% and -8.7% of *PIC* concentrations determined from satellite data with respect to those from AERONET-OC data, thus further confirming the potential for current satellite data products in quantifying *PIC* concentrations.

Declaration of Competing Interest

The authors declare that they have no known competing financial interests or personal relationships that could have appeared to influence the work reported in this paper.

Acknowledgments

The authors would like to thank NASA OBPG for granting access to the MODIS and VIIRS data, EUMETSAT for providing the OLCI data and the AERONET Team for processing and distributing the data from the Ocean Color component of the Aerosol Robotic Network.

Special acknowledgments are due to Violeta Slabakova and Dragos Niculescu for their invaluable help in maintaining the Galata and Gloria/Section-7 sites, respectively.

References

Ahmad, Z., Franz, B.A., McClain, C.R., Kwiatkowska, E.J., Werdell, J., Shettle, E.P., Holben, B.N., 2010. New aerosol models for the retrieval of aerosol optical thickness and normalized water-leaving radiances from the SeaWiFS and MODIS sensors over coastal regions and open oceans. Appl. Opt. 49, 5545–5560. https://doi.org/10.1364/AO.49.005545.

Antoine, D., 2010. Sentinel-3 optical products and algorithm definition. In: OLCI Level 2 Algorithm Theoretical Basis Document: Ocean Color Products in case 1 waters - Ref. S3-L2-SD-03- C10-LOV-ATBD.

Aubrey, D., Moncheva, S., Demirov, E., Diaconu, V., Dimitrov, A., 1996. Environmental changes in the western Black Sea related to anthropogenic and natural conditions. J. Mar. Syst. 7, 411–425. https://doi.org/10.1016/0924-7963(95)00031-3.

Bailey, S.W., Franz, B.A., Werdell, P.J., 2010. Estimation of near-infrared water-leaving reflectance for satellite ocean color data processing. Opt. Express 18, 7521. https://doi.org/10.1364/oe.18.007521.

Balch, W.M., Gordon, H.R., Bowler, B.C., Drapeau, D.T., Booth, E.S., 2005. Calcium carbonate measurements in the surface global ocean based on Moderate-Resolution Imaging Spectroradiometer data. J. Geophys. Res. C Ocean 110, 1–21. https://doi.org/10.1029/2004JC002560.

Balch, W.M., Drapeau, D.T., Bowler, B.C., Lyczskowski, E., Booth, E.S., Alley, D., 2011. The contribution of coccolithophores to the optical and inorganic carbon budgets during the Southern Ocean Gas Exchange Experiment: new evidence in support of the Great Calcite Belt hypothesis. J. Geophys. Res. Ocean 116, 1–14. https://doi.org/10.1029/2011JC006941.

Baith, K., Lindsay, R., Fu, G., McClain, C.R., 2001. Data analysis system developed for ocean color satellite sensors. Eos. Trans. Am. Geophys. Union 82, 202. https://doi.org/10.1029/01EO00109.

Balch, W.M., Bowler, B.C., Drapeau, D.T., Lubelczyk, L.C., Lyczkowski, E., 2018. Vertical distributions of Coccolithophores, PIC, POC, Biogenic Silica, and Chlorophyll a throughout the Global Ocean. Glob. Biogeochem. Cycles 32, 2–17. https://doi.org/10.1002/2016GB005614.

Brown, C.W., Yoder, J.A., 1994. Coccolithophorid blooms in the global ocean. J. Geophys. Res. 99, 7467–7482. https://doi.org/10.1029/93JC02156.

Clark, D.K., Murphy, M., Yarbrough, M., Feinholz, M., Flora, S., Broenkow, W., Johnson, B., Brown, S., Kim, Y., Mueller, J., 2003. MOBY, A Radiometric Buoy for Performance Monitoring and Vicarious Calibration of Satellite Ocean Color Sensors: Measurement and Data Analysis Protocols. In: SeaWiFs Postlaunch Technical Report Series (Accessed June 4, 2021).

Cokacar, T., Kubilay, N., Oguz, T., 2001. Structure of Emiliania huxleyi blooms in the Black Sea surface waters as detected by Sea WIFS imagery. Geophys. Res. Lett. 28, 4607–4610. https://doi.org/10.1029/2001GL013770.

Cokacar, T., Oguz, T., Kubilay, N., 2004. Satellite-detected early summer coccolithophore blooms and their interannual variability in the Black Sea. Deep. Res. Part I Oceanogr. Res. Pap. 51, 1017–1031. https://doi.org/10.1016/j.dsr.2004.03.007.

Donlon, C., Berruti, B., Buongiorno, A., Ferreira, M.-H., Féménias, P., Frerick, J., Goryl, P., Klein, U., Laur, H., Mavrocordatos, C., Nieke, J., Rebhan, H., Seitz, B., Stroede, J., Sciarra, R., 2012. The Global Monitoring for Environment and Security (GMES) Sentinel-3 mission. Remote Sens. Environ. 120, 37–57. https://doi.org/10.1016/j.rse.2011.07.024.

Esaias, W.E., Abbott, M.R., Barton, I., Brown, O.B., Campbell, J.W., Carder, K.L., Clark, D.K., Evans, R.H., Hoge, F.E., Gordon, H.R., Balch, W.M., Letelier, R., Minnett, P.J., 1998. An overview of MODIS capabilities for ocean science observations. IEEE Trans. Geosci. Remote Sens. 36, 1250–1265. https://doi.org/10.1109/36.701076.

EUMETSAT, 2017. Sentinel-3A Product Notice – OLCI Level-2 Ocean Colour. EUM/OPS-SEN3/DOC/17/928907, https://www-cdn.eumetsat.int/files/2020-04/pdf_s3a_pn_olci_l2_rep.pdf. Last accessed on 2021 June 3rd.

EUMETSAT, 2018. Sentinel-3A product notice – OLCI Level-2 Ocean Colour Operational Products and Full-Mission Reprocessed Time Series. EUM/OPS-SEN3/DOC/17/964713, https://www-cdn.eumetsat.int/files/2020-04/pdf_s3a_pn_olci_l2_rep.pdf. Last accessed on 2021 March 3rd.

Franz, B.A., Bailey, S.W., Werdell, P.J., McClain, C.R., 2007. Sensor-independent approach to the vicarious calibration of satellite ocean color radiometry. Appl. Opt. 46, 5068–5082. https://doi.org/10.1364/AO.46.005068.

Garcia, C.A.E., Garcia, V.M.T., Dogliotti, A.I., Ferreira, A., Romero, S.I., Mannino, A., Souza, M.S., Mata, M.M., 2011. Environmental conditions and bio-optical signature of a coccolithophorid bloom in the Patagonian shelf. J. Geophys. Res. Ocean 116. https://doi.org/10.1029/2010JC006595.

Gergely, M., Zibordi, G., 2014. Assessment of AERONET-OC LWN uncertainties. Metrologia 51, 40–47. https://doi.org/10.1088/0026-1394/51/1/40.

Goldberg, M.D., Kilcoyne, H., Cikanek, H., Mehta, A., 2013. Joint Polar Satellite System: the United States next generation civilian polar-orbiting environmental satellite system. J. Geophys. Res. Atmos. 118, 13,413–463,475. https://doi.org/10.1002/2013JD020389.

Gordon, H.R., Wang, M., 1994. Retrieval of water-leaving radiance and aerosol optical thickness over the oceans with SeaWiFS: a preliminary algorithm. Appl. Opt. 33, 443–452. https://doi.org/10.1364/AO.33.000443.

Gordon, H.R., Boynton, G.C., Balch, W.M., Groom, S.B., Harbour, D.S., Smyth, T.J., 2001. Retrieval of coccolithophore calcite concentration from sea WiFS imagery. Geophys. Res. Lett. 28, 1587–1590. https://doi.org/10.1029/2000GL012025.

Groom, S.B., Holligan, P.M., 1987. Remote sensing of coccolithophore blooms. Adv. Sp. Res. 7, 73–78. https://doi.org/10.1016/0273-1177(87)90166-9.

Holligan, P.M., Balch, W.M., 1991. From the ocean to cells: coccolithophore optics and biogeochemistry. NATO ASI Ser. Part. Anal. Oceanogr. G 27, 301–324.

Hopkins, J., Henson, S.A., Painter, S.C., Tyrrell, T., Poulton, A.J., 2015. Phenological characteristics of global coccolithophore blooms. Glob. Biogeochem. Cycles 29, 239–253. https://doi.org/10.1002/2014GB004919.

Iglesias-Rodríguez, M.D., Brown, C.W., Doney, S.C., Kleypas, J., Kolber, D., Kolber, Z., Hayes, P.K., Falkowski, P.G., 2002. Representing key phytoplankton functional groups in ocean carbon cycle models: coccolithophorids. Glob. Biogeochem. Cycl. 16 https://doi.org/10.1029/2001gb001454, 47-1-47-20.

Iida, T., Saitoh, S.I., Miyamura, T., Toratani, M., Fukushima, H., Shiga, N., 2002. Temporal and spatial variability of coccolithophore blooms in the eastern Bering

Sea, 1998–2001. Prog. Oceanogr. 55, 165–175. https://doi.org/10.1016/S0079-6611(02)00076-9.
Karabashev, G.S., Sheberstov, S.V., Yakubenko, V.G., 2006. The June maximum of normalized radiance and its relation to the hydrological conditions and coccolithophorid bloom in the Black Sea. Oceanology 46, 305–317. https://doi.org/10.1134/S0001437006030027.
Kopelevich, O., Burenkov, V., Sheberstov, S., Vazyulya, S., Kravchishina, M., Pautova, L., Silkin, V., Artemiev, V., Grigoriev, A., 2014. Satellite monitoring of coccolithophore blooms in the Black Sea from ocean color data. Remote Sens. Environ. 146, 113–123. https://doi.org/10.1016/j.rse.2013.09.009.
Kopelevich, O., Sheberstov, S., Vazyulya, S., 2020. Effect of a coccolithophore bloom on the underwater light field and the albedo of the water column. J. Mar. Sci. Eng. https://doi.org/10.3390/jmse8060456.
Korchemkina, E.N., Mankovskaya, E.V., Sea, B., 2019. Bio-optical properties of Black Sea in July 2017. In: Proc. SPIE 11208, 25th International Symposium on Atmospheric and Ocean Optics: Atmospheric Physics. https://doi.org/10.1117/12.2540813.
Kubryakov, A.A., Mikaelyan, A.S., Stanichny, S.V., 2019. Summer and winter coccolithophore blooms in the Black Sea and their impact on production of dissolved organic matter from Bio-Argo data. J. Mar. Syst. 199, 103220. https://doi.org/10.1016/j.jmarsys.2019.103220.
Mélin, F., Zibordi, G., Berthon, J.-F., Bailey, S., Franz, B., Voss, K., Flora, S., Grant, M., 2011. Assessment of MERIS reflectance data as processed with SeaDAS over the European seas. Opt. Express 19, 25657–25671. https://doi.org/10.1364/OE.19.025657.
Mitchell, C., Hu, C., Bowler, B., Drapeau, D., Balch, W.M., 2017. Estimating particulate inorganic carbon concentrations of the global ocean from ocean color measurements using a reflectance difference approach. J. Geophys. Res. Ocean 122, 8707–8720. https://doi.org/10.1002/2017JC013146.
Moore, G., Lavender, S., 2010. OLCI Bright Waters AC (mesotrophic to high turbidity). Algorithm Theoretical Basis Document. S3-L2-SD-03-C08-ARGATBD_BWAC. https://sentinel.esa.int/documents/247904/349589/OLCI_L2_ATBD_Atmospheric_Corrections_Bright_Waters.pdf. Last accessed on 2021 March 3rd.
Moore, T.S., Dowell, M.D., Franz, B.A., 2012. Detection of coccolithophore blooms in ocean color satellite imagery: a generalized approach for use with multiple sensors. Remote Sens. Environ. 117, 249–263. https://doi.org/10.1016/j.rse.2011.10.001.
Morel, A., Antoine, D., Gentili, B., 2002. Bidirectional reflectance of oceanic waters: accounting for Raman emission and varying particle scattering phase function. Appl. Opt. 41, 6289–6306. https://doi.org/10.1364/AO.41.006289.
Müller, M.N., 2019. On the genesis and function of coccolithophore calcification. Front. Mar. Sci. 6, 49. https://doi.org/10.3389/fmars.2019.00049.
Neukermans, G., Fournier, G., 2018. Optical modeling of spectral backscattering and remote sensing reflectance from Emiliania huxleyi Blooms. Front. Mar. Sci. 5, 1–20. https://doi.org/10.3389/fmars.2018.00146.
Schueler, C.F., Clement, J.E., Ardanuy, P.E., Welsch, C., DeLuccia, F., Swenson, H., 2002. NPOESS VIIRS sensor design overview. In: Barnes, W.L. (Ed.), Earth Observing Systems VI. SPIE, pp. 11–23. https://doi.org/10.1117/12.453451.
Slabakova, V., Moncheva, S., Slabakova, N., Dzhembekova, N., 2020. Evaluation of sentinel-3a olci ocean color products in the Western Black Sea. In: Proceeding of 1st International Conference on Environmental Protection and Disaster RISKs, pp. 271–281. https://doi.org/10.48365/ENVR-2020.1.25.
Smyth, T.J., Moore, G.F., Groom, S.B., Land, P.E., Tyrrell, T., 2002. Optical modeling and measurements of a coccolithophore bloom. Appl. Opt. 41, 7679. https://doi.org/10.1364/ao.41.007679.
Stagl, J.C., Hattermann, F.F., 2015. Impacts of climate change on the hydrological regime of the Danube river and its tributaries using an ensemble of climate scenarios. Water 7, 6139–6172. https://doi.org/10.3390/w7116139.
Thierstein, H.R., Young, J.R., 2013. Coccolithophores: From Molecular Processes to Global Impact. Springer, Berlin Heidelberg.
Thuillier, G., Hersé, M., Labs, D., Foujols, T., Peetermans, W., Gillotay, D., Simon, P.C., Mandel, H., 2003. The solar spectral irradiance from 200 to 2400 nm as measured by the SOLSPEC spectrometer from the atlas and Eureca missions. Sol. Phys. 214, 1–22. https://doi.org/10.1023/A:1024048429145.
Vespremeanu, E., Golumbeanu, M., 2018. Catchment area of the Black Sea. In: The Black Sea: Physical, Environmental and Historical Perspectives. Springer International Publishing, Cham, pp. 15–25. https://doi.org/10.1007/978-3-319-70855-3_3.
Zibordi, G., Mélin, F., Berthon, J.-F., Holben, B., Slutsker, I., Giles, D., D'Alimonte, D., Vandemark, D., Feng, H., Schuster, G., Fabbri, B.E., Kaitala, S., Seppälä, J., 2009. AERONET-OC: a network for the validation of ocean color primary products. J. Atmos. Ocean. Technol. 26, 1634–1651. https://doi.org/10.1175/2009JTECHO654.1.
Zibordi, G., Mélin, F., Berthon, J.F., Talone, M., 2015. In situ autonomous optical radiometry measurements for satellite ocean color validation in the Western Black Sea. Ocean Sci. 11, 275–286. https://doi.org/10.5194/os-11-275-2015.
Zibordi, G., Holben, B.N., Talone, M., D'Alimonte, D., Slutsker, I., Giles, D.M., Sorokin, M.G., 2021. Advances in the ocean color component of the aerosol robotic network (AERONET-OC). J. Atmos. Ocean. Technol. https://doi.org/10.1175/JTECH-D-20-0085.1.